Population dynamics of choice representation in dorsal premotor and primary motor cortex

Diogo Peixoto[1,2]*, Roozbeh Kiani[3], Chandramouli Chandrasekaran[4,5], Stephen I. Ryu[4,6], Krishna V. Shenoy[1,4,5,7,8,9], William T. Newsome[1, 5,7, 8]

1 Neurobiology Department, Stanford University, Stanford, CA, USA, 94305

2 Champalimaud Neuroscience Programme, Lisbon, Portugal, 1400-038

3 Center for Neural Science, New York University, New York, NY, USA, 10003

4 Electrical Engineering Department, Stanford University, Stanford, CA, USA

5 Howard Hughes Medical Institute, Stanford University, CA, USA, 94305

6 Palo Alto Medical Foundation, Palo Alto, California, CA, USA, 94301

7 Stanford Neurosciences Institute, Stanford University, CA, USA, 94305

8 Bio-X program, Stanford University, CA, USA, 94305

9 Bioengineering Department, Stanford University, Stanford, CA, USA, 94305

Please address correspondence to Bill Newsome (bnewsome@stanford.edu) or Diogo Peixoto (dpeixoto@stanford.edu)

Summary

Studies in multiple species have revealed the existence of neural signals that lawfully co-vary with different aspects of the decision-making process, including choice, sensory evidence that supports the choice, and reaction time. These signals, often interpreted as the representation of a decision variable (DV), have been identified in several motor preparation circuits and provide insight about mechanisms underlying the decision-making process. However, single-trial dynamics of this process or its representation at the neural population level remain poorly understood. Here, we examine the representation of the DV in simultaneously recorded neural populations of dorsal premotor (PMd) and primary motor (M1) cortices of monkeys performing a random dots direction discrimination task with arm movements as the behavioral report. We show that single-trial DVs covary with stimulus difficulty in both areas but are stronger and appear earlier in PMd compared to M1 when the stimulus duration is fixed and predictable. When temporal uncertainty is introduced by making the stimulus duration variable, single-trial DV dynamics are accelerated across the board and the two areas become largely indistinguishable throughout the entire trial. These effects are not trivially explained by the faster emergence of motor kinematic signals in PMd and M1. All key aspects of the data were replicated by a computational model that relies on progressive recruitment of units with stable choice-related modulation of neural population activity. In contrast with several recent results in rodents, decision signals in PMd and M1 are not carried by short sequences of activity in non-overlapping groups of neurons but are instead distributed across many neurons, which once recruited, represent the decision stably during individual behavioral epochs of the trial.

43 **Introduction**
44
45 When navigating in traffic, a driver constantly integrates evidence about the outside
46 world that must inform upcoming decisions: stay on the throttle, press the brake,
47 switch gears, etc. This process of deliberating on available sensory evidence to reach
48 a commitment to a specific proposition or action is termed perceptual decision-
49 making (Hanks and Summerfield, 2017, Brody and Hanks, 2016, Murakami and
50 Mainen, 2015, Shadlen and Kiani, 2013, Gold and Shadlen, 2007). In the driver
51 example, the actions involve limb movements, and in such contexts, primary motor
52 cortex (M1) and dorsal premotor cortex (PMd) are thought to be involved in the
53 decision-making process (Guo et al., 2014, Thura and Cisek, 2014, Cisek, 2012, Cisek
54 and Kalaska, 2010, Cisek, 2007, Cisek and Kalaska, 2005, Wise, 1985, Vaadia et al.,
55 1988, Wise et al., 1997). In particular, lesion (Passingham, 1985), inactivation
56 (Kurata and Hoffman, 1994, Sasaki and Gemba, 1986) and electrophysiological
57 studies (Cisek and Kalaska, 2005, Song and McPeek, 2010, Hoshi, 2013) suggest an
58 important role for PMd and M1 in action selection and visuomotor association.
59 Recent studies have employed more sophisticated perceptual discrimination tasks
60 with arm movements as the operant response (Thura and Cisek, 2014,
61 Chandrasekaran et al., 2017, Coallier et al., 2015) and shown that firing rates of a
62 diverse neural population in PMd covaries with choice, stimulus difficulty, and
63 reaction time (RT) well before the movement onset. These results are consistent with
64 a role for PMd and M1 in "somatomotor" decisions and also suggest the presence of a
65 candidate DV, organized by cortical laminae, in these brain areas (Thura and Cisek,
66 2014, Thura and Cisek, 2016, Coallier et al., 2015, Palmer et al., 2005, Wang et al.,
67 2016, Chandrasekaran et al., 2017).
68
69 With few exceptions (Bollimunta et al., 2012, Kaufman et al., 2015, Kiani et al.,
70 2014b, Ponce-Alvarez et al., 2012, Rich and Wallis, 2016), neurophysiological
71 studies of decision mechanisms have focused on *average* decision-related signals at
72 the single neuron level (Roitman and Shadlen, 2002, Churchland et al., 2008, Kiani
73 and Shadlen, 2009, de Lafuente et al., 2015) and at the population level (Mante et al.,
74 2013, Machens et al., 2010, Raposo et al., 2014). Key questions remain unanswered
75 about the single-trial dynamics and spatiotemporal structure of neural population
76 responses in perceptual decision formation in PMd and M1. We therefore trained
77 macaque monkeys to perform fixed as well as variable-duration random-dot motion
78 direction discrimination tasks (Kiani et al., 2008) using an arm movement as the
79 operant response while simultaneously recording hundreds of neurons using Utah
80 arrays implanted in PMd and M1. We used decoding techniques to estimate single-
81 trial DVs from PMd and M1 firing rates, and examined how the dynamics of these
82 decoded DVs changed with parameters such as stimulus difficulty and uncertainty
83 about expected stimulus duration. Our analyses focused on three interconnected
84 questions.
85
86 First, we analyzed the relationship between single-trial dynamics of the DV and
87 sensory stimuli that inform the choice, and determined whether these dynamics differ
88 between PMd and M1. We then tested whether the neural dynamics change when
89 subjects transition from a context of temporal certainty to high temporal uncertainty
90 about stimulus duration (Shadlen and Newsome, 2001, Murphy et al., 2016).
91
92 Second, we used computational modeling of behavior and neural responses to identify

93   mechanisms that can explain the observed dynamics of choice representation in PMd
94   and M1 under different task conditions. Bounded accumulation of evidence is a
95   widely used modeling framework for perceptual decisions in the direction
96   discrimination and similar sensory tasks (Ratcliff and McKoon, 2007). For a binary
97   choice, the model assumes that two accumulators integrate sensory evidence in favor
98   of the two competing options until one of the accumulators reaches a decision
99   threshold or bound (Vickers, 1970, Link, 1992, Beck et al., 2008, Shadlen and Kiani,
100   2013, Kiani et al., 2014a). We considered three variants of this model that could offer
101   a theoretical account for accelerated representation of choice under temporal
102   uncertainty: increased urgency or reduced bound (Churchland et al., 2008, Heitz and
103   Schall, 2012, Purcell and Kiani, 2016, Hanks et al., 2014), increased input gain (Cisek
104   et al., 2009, Thura et al., 2012), and a novel framework based on progressive
105   recruitment of choice representing neurons which suggests that the fraction of neurons
106   carrying choice related signals increases throughout the trial, leading to increasingly
107   more stable choice representation over the course of the trial.
108
109   Our final goal was to understand how a stable choice representation is implemented
110   by a population of PMd and M1 neurons. We considered two competing hypotheses:
111   sustained representation of choice by: 1) a stable population of neurons, or 2) a
112   sequence of transient responses in non-overlapping groups of neurons. Sustained
113   responses are commonly observed in the frontoparietal cortex of the primate brain and
114   are implicated as a substrate for working memory, decision-making, and higher
115   cognitive functions (Chandrasekaran et al., 2017, Churchland et al., 2008, Cisek and
116   Kalaska, 2005, Kiani and Shadlen, 2009, Machens et al., 2010, Mante et al., 2013,
117   Roitman and Shadlen, 2002, Shadlen and Newsome, 2001, Thura and Cisek, 2014,
118   Goldman-Rakic, 1995). An alternative mechanism has recently emerged from optical
119   imaging studies in rodents (Harvey et al., 2012, Morcos and Harvey, 2016) and later
120   expanded to electrophysiological and computational studies (Rajan et al., 2016, Scott
121   et al., 2017), suggesting that decision-related activity may be carried by transient
122   sequences of small subsets of neurons at different points in time. The "sequence"
123   model predicts that in a given epoch in the trial, only a small subset of neurons
124   represents the decision, and this subset will be largely non-overlapping with the
125   subset of decision related neurons for any other epoch in the trial.
126
127   We found that, in the fixed duration task, single-trial DVs are represented in both
128   PMd and M1 shortly after stimulus onset but are stronger and faster in PMd compared
129   to M1. On single trials, estimated DVs exhibit ramp-like growth during stimulus
130   presentation and the slope is steeper for easier coherences compared to harder
131   coherences. In the variable duration task, for both PMd and M1, DV dynamics are
132   strikingly accelerated and are nearly identical in the two areas throughout the entire
133   trial, although PMd responses still lead M1 responses by ~15 ms. Even though single
134   trial DVs ramp up faster in the variable-duration task, the co-variation of ramp slope
135   with stimulus difficulty was preserved and behavioral accuracy remained largely
136   stable. Control analyses show that these results are not explained by accelerated
137   representation of motor variables such as reach speed, other kinematics of the arm and
138   eye, or eventual RT, nor could the combined physiological and behavioral data be
139   modeled accurately by changes in gain or urgency. Instead, the data are consistent
140   with a progressive recruitment of choice-related neurons that is accelerated under
141   uncertainty conditions. Consistent with the progressive recruitment model, the
142   empirically observed population choice signals become increasingly stable throughout

143 the stimulus presentation as more units with sustained choice selectivity are recruited.
144 This stabilization happens more rapidly in the variable duration task, in which there is
145 a high premium for quick decisions (Murphy et al., 2016).
146
147

Results

148

149

150 **Monkeys discriminate stimulus motion better for higher coherence and longer**
151 **duration trials**

152

153 We trained monkeys in a variant of the classical random dot motion discrimination
154 task (RDM, (Britten et al., 1992)), in which animals report the net direction of motion
155 in a random dot kinematogram (Shadlen and Newsome, 2001, Kiani et al., 2008,
156 Britten et al., 1992) presented on a LCD touchscreen (Fig. 1a). In our variant of the
157 RDM task, the monkeys used an arm reach to one of two targets corresponding to the
158 perceived direction of motion to report their decision (Fig. 1a-b). In the fixed
159 duration version of the task the stimulus was always presented for 1000 ms followed
160 by a random delay period (400-900 ms) after which the monkey was provided with a
161 "go cue" to report its decision. Eye fixation was enforced from the beginning of the
162 trial until appearance of the go cue to impose additional behavioral control and avoid
163 interpretational confounds since PMd activity can be modulated by eye-hand relative
164 position (Pesaran et al., 2006).

165

166 Monkeys displayed excellent behavioral performance in this task, achieving close to
167 ceiling levels of accuracy (99% for both monkeys) for the highest coherence stimuli
168 (Fig. 1c, black curves). The accuracy decreased smoothly with stimulus difficulty
169 (lower coherence) and remained above chance for the lowest (non-zero) coherence
170 stimulus (3.2% coherence, 59%-62% accuracy for monkey H-F). Psychophysical
171 thresholds (α) (estimated at 81.6% accuracy by fitting a cumulative Weibull function
172 to the performance curves) were 12.1% and 12.4% stimulus coherence for monkey H
173 and F, respectively (Fig.1c, black dashed vertical lines).

174

175 After data collection was concluded in the fixed duration task, monkeys performed a
176 variable duration RDM task, (Fig. 1c, red curves). In these experiments, stimulus
177 duration was randomly selected on each trial (200-1000 ms exponentially distributed,
178 median 435 ms) and the delay period was eliminated, requiring subjects to report their
179 decision immediately after stimulus offset. Psychophysical thresholds for both
180 monkeys decreased as stimulus duration increased up to ~500 msec (Fig. 1d)
181 indicating that monkeys performed better for longer stimuli. This improvement in
182 performance suggests that additional visual evidence was utilized to improve
183 decisions as a result of integrating the sensory evidence for a longer duration. The
184 improvement in thresholds occurred at the rate expected from a perfect integrator
185 model (slope, ~ -0.5) for stimulus durations up to approximately 533 and 682 ms for
186 monkey H and F, respectively, with little or no improvement for longer stimuli (Kiani
187 et al., 2008, Kiani and Shadlen, 2009).

188

189 The two tasks enabled us to probe the dynamics of decision-related signals in
190 PMd/M1. The fixed duration task provided temporal separation between evidence
191 integration (dots period), action planning (hold period), and action execution (post-go
192 period). In contrast, the variable duration task provided the ability to query the

193   subject's choice as soon as the stimulus is terminated.
194
195   **Single trial choice signals in PMd and M1 are compatible with the neural**
196   **representation of a decision variable**
197
198   We recorded neural activity in PMd and M1, using two chronically implanted 96-
199   channel Utah arrays (Fig. 1e), while subjects performed each motion discrimination
200   task. Consistent with prior studies in PMd (Cisek and Kalaska, 2005, Chandrasekaran
201   et al., 2017), we found diverse responses at the single cell level, which may reflect
202   multiple functions being implemented in this area (Supp. Fig. 1). The same
203   observation was true for M1 (Supp. Fig. 2).
204
205   Our primary goal was to understand the dynamics of these diverse neural responses in
206   PMd and M1 at the population level—both on average and on single trials. We trained
207   a regularized logistic classifier to predict right and left choices on individual trials
208   based on short periods of neural activity (50 ms windows), using a method we
209   developed in a recent study (Kiani et al., 2014b). Classification was based on features
210   of the simultaneously recorded activity from ~100-200 units from each area (Kiani et
211   al., 2014b) (median number of units/session: 153 for PMd, 147 for M1).
212
213   For the fixed duration task, choice prediction accuracy before and immediately after
214   the onset of the targets was near chance (Fig. 2a, Supp. Fig. 3a and 4a) suggesting that
215   choice biases prior to motion onset were negligible and the monkey's choices were
216   shaped by the motion stimulus. Choice prediction accuracy rose above chance at 187
217   ± 12 ms (mean±s.d.) after stimulus onset for PMd and 240 ± 14 ms (mean±s.d.) for
218   M1. The median latencies for PMd were significantly shorter than for M1 (Wilcoxon
219   rank sum test, p<0.001) and were similar to other reports of decision-related signals in
220   PMd (Thura and Cisek, 2014, Chandrasekaran et al., 2017) and MIP (de Lafuente et
221   al., 2015). Although our monkeys were extensively trained on this version of the task
222   that allowed them 1000 msec to evaluate the stimulus motion and at least another 400
223   msec of delay period to prepare the operant response, both PMd and M1 still
224   responded in a choice predictive manner less than 250 ms after the stimulus onset and
225   over a second before the initiation of the action was cued. Thus, choice predictive
226   activity in these (pre)motor structures, similar to their parietal counterparts (Shadlen
227   and Newsome, 2001) is not contingent on having to prepare for immediate action, but
228   is also present when that action is delayed ~1-2 seconds into the future.
229
230   Choice prediction accuracy rose steadily for both areas as the trial proceeded, but was
231   significantly higher for PMd than for M1 (P<0.05 Wilcoxon Sign rank test, Holm-
232   Bonferroni corrected) during most of the motion-viewing epoch (Fig. 2a, Supp. Fig.
233   3a and 4a). This difference was observed in both monkeys and did not result from a
234   higher number of recorded units in PMd (Wilcoxon rank sum test comparing median
235   number of units, p=0.41). At the end of the visual stimulus period prediction accuracy
236   reached 84.5% ± 1.3% and 83% ± 0.5% (mean±s.e.m.) for PMd and 72% ± 0.9% and
237   78% ± 0.9% (mean±s.e.m.) for M1 of monkeys H and F, respectively (Fig. 2a; Supp.
238   Fig. 3a and 4a). These classification accuracies roughly matched (in M1) or exceeded
239   (in PMd) those previously reported for neural population recordings in prearcuate
240   cortex using similar recording and analysis techniques (Kiani et al., 2014b) (and could
241   be even further increased by adjusting the window size Supp. Fig. 5), confirming the
242   possibility of obtaining single trial read-outs of a decision state from these areas.

5

243

244 Highly reliable choice predictive activity with short latencies is expected from
245 standard accumulation-to-bound models of decision formation (Mazurek, 2003, Cisek
246 et al., 2009). The second expectation is that the rate of increase of choice predictive
247 activity should depend on stimulus difficulty (Gold and Shadlen, 2007). Consistent
248 with this expectation, classification accuracy on easier trials rose faster and attained
249 higher values compared to harder trials (Fig. 2b-c, Supp. Fig. 3b-c and 4b-c). This
250 feature was present in both areas though the separation between stimulus difficulties
251 was stronger in PMd than M1 between 200-600 ms aligned to stimulus onset
252 (Wilcoxon sign rank test, P<0.005, Supp. Fig. 6). The third expectation is that the
253 relationship between classification accuracy and motion coherence be stronger during
254 the first half of the dots period and becomes smaller as the trial unfolds (Shadlen and
255 Newsome, 2001, Roitman and Shadlen, 2002, Kiani et al., 2008, Wang, 2002) (Supp.
256 Fig. 6, 200-600 vs 600-1000 ms periods). Finally, during the delay and peri-
257 movement periods prediction accuracy is high with little or no separation by stimulus
258 difficulty, suggesting that a categorical decision is made by the end of the delay
259 period in the vast majority of trials. Overall, the dynamics of the choice prediction
260 accuracy matched accumulation of evidence and commitment to a choice when
261 adequate evidence was accumulated.

262

263 To better understand the dynamics of decision-related activity, we calculated a
264 continuous readout of the strength of the model's prediction for the subject's choice,
265 which is critical for single trial analyses to follow. We calculated the logistic model's
266 log odds ratio for the two choices for each time point on every trial. This variable is
267 equal to the distance of the neural population activity from the classifying hyperplane
268 (Supp. Fig. 7a). As in our previous study (Kiani et al., 2014b), we interpreted this
269 distance as the model's decision variable (DV) and used it as a proxy for the internal
270 cognitive state of the animal, representing a preference for a given choice. Because
271 the DV is continuous (unlike predicted choice which is binary) and can differ even
272 between correctly predicted trials (Supp. Fig. 7a), it provided a continuous metric for
273 quantifying the internal cognitive state and its dependency on stimulus difficulty. Our
274 convention was that positive values of the DV reflect increased likelihood of right
275 choices and negative values reflect left choices. As expected the average decision
276 variable showed the same effects found for choice prediction accuracy: (i) its
277 magnitude increases with time and with stimulus coherence (Supp. Fig. 7b), (ii) the
278 coherence-dependent separation of the DVs depends on the time in the motion
279 viewing period, and (iii) this separation vanishes around the time of Go cue and motor
280 response.

281

282 We next investigated whether these effects of stimulus difficulty held on *single trials*.
283 If the DV traces truly ramped up on single trials, their slopes should increase as a
284 function of coherence. Alternatively, if the entire system synchronously stepped from
285 an uncertain state to a committed state at different points in time for different trials
286 (with ramping being an artifact of averaging multiple trials) the slopes should not
287 depend on stimulus coherence. Our results cannot exclude the possibility that
288 population-level ramping is implemented by asynchronously stepping neurons
289 (Latimer et al., 2015) whose step times are coherence dependent.

290

291 To quantify stimulus coherence effects on the single-trial DV we focused on the first
292 half of the stimulus presentation interval (500 msec). This time window was

6

293   consistent with a conservative estimate of the motion integration times from
294   psychophysical data for both monkeys (Fig. 1d). We used a tri-linear fit to single-trial
295   DV traces. The fitted function consisted of an initial interval of zero slope, reflecting
296   the finite latency between dots onset and initial modulation of PMd/M1 activity. The
297   slope during the second interval captures a period of rapid DV change following dots
298   onset, while the third interval reflects a general slowing of DV change that occurs by
299   the middle of the dots period (Supp. Fig. 7b-d, see Methods). The tri-linear fit enables
300   us to focus on the rate of rise of the DV during decision-making (Shadlen et al.,
301   2016). Consistent with the ramping representation, at the population level, of a
302   decision variable on single trials in these areas, higher coherence trials are associated
303   with steeper DV slopes (second slope of the tri-linear fits, Figure 2d-e, Supp. Fig. 3d-
304   e and Supp. Fig. 4d-e). The results are significant for both areas and choice directions
305   (for both models: slope vs coherence and slope vs $\log_2$(coherence); see Methods,
306   statistical analyses Supp. Table 1).

307
**Stimulus duration uncertainty increases and accelerates choice predictive
activity in both areas**

310
311   So far, we focused on the neural activity from the fixed duration task for which the
312   animals consistently had 1 second of visual evidence to deliberate and decide upon.
313   However, in the real world, subjects rarely know the precise timing of visual
314   information relevant to making a choice. Thus, after experiments on the fixed
315   duration task, we introduced the variable duration task and trained the monkeys to
316   report their decision immediately upon termination of the stimulus (Fig. 1a,b;
317   Methods). Prior to these recordings the monkeys had never been exposed to short
318   duration stimuli (< 1000 ms).

319
320   Since subjects could not predict the duration of the stimulus on single trials and most
321   trials were short (median 435 ms, see Methods), the variable-duration task
322   incentivized accurate assessment of sensory evidence early in the stimulus
323   presentation period: the first 200 ms of dots motion were guaranteed to be shown but
324   stimulus presentation could be terminated at any point thereafter. We asked whether
325   the dynamics of decision-related signals in PMd and M1 were different in the variable
326   duration task. In both areas, we found that classification accuracy increased faster in
327   the variable duration task leading to much higher accuracy values during the stimulus
328   presentation period (Fig. 3a, Supp. Fig. 8a, Supp. Fig. 9a). This acceleration in
329   prediction accuracy was most apparent in M1, where choice predictive neural
330   responses emerged much faster in the variable duration task (193 ± 12 ms compared
331   to 240 ± 14 ms in the fixed duration task). This earlier onset also happened in PMd
332   (177 ± 8 ms compared to 187 ± 12 ms in the fixed duration task), though to a lesser
333   extent. Consequently, the difference in the onset time of choice-related activity
334   between PMd and M1 diminished substantially in the variable duration task (latency
335   difference= 13.2 ms in variable duration versus 41.6 ms in fixed duration task, p=1.6
336   x 10^{-13}, Wilcoxon rank sum test). Moreover, the difference in absolute prediction
337   accuracy between the two areas was significant for only 80 ms during the entire dots
338   period (P<0.05 Wilcoxon Rank Sum test, Holm-Bonferroni corrected), confirming
339   that these areas represent the upcoming choice with very similar strength in the
340   variable duration task.

341
342   The slope analysis of single-trial DVs in the variable duration task showed that the

343 coherence effects were largely conserved on single trials in both PMd and M1 despite
344 the accelerated dynamics (dashed lines in Fig. 3b-c, Supp. Fig. 8b-c, Supp. Fig. 9b-c,
345 statistical analyses, Supp. Table 1, all parameters, Supp. Fig 10 Supp. Fig 11). The
346 DV slopes are overall larger for the variable duration task compared to the fixed
347 duration task (vertical shift between the solid and dashed lines in Fig. 3b-c, Supp. Fig.
348 8b-c, Supp. Fig. 9b-c). This difference was significant for all areas and target
349 directions ($p < 10^{-18}$, see Methods and Supp. Table 4).
350
351 **Changes in decision-related dynamics are not due to contamination by motor**
352 **signals**
353
354 The data in Fig. 3b,c suggested that dynamics of decision-related activity accelerated
355 under conditions of temporal uncertainty, as indicated by the overall larger slopes in
356 the variable duration task. Before testing model predictions, we addressed a potential
357 confound that could lead to misinterpretation of the DV slope data. When the
358 duration of the stimulus is uncertain and the operant response is required immediately
359 after offset of the stimulus (i.e. no delay period), it is possible that motor planning is
360 accelerated and that kinematic signals related to the operant movement invade the
361 visual stimulus period, contaminating our DV estimates from PMd and M1
362 recordings. If the accelerated dynamics were exclusively due to motor preparation
363 signals contaminating the early dots period, we would expect the coherence effects on
364 single trial DVs to diminish or disappear altogether in the variable duration task. This
365 was not the case as shown in Figures 3b-c, Supplementary Figures 8b-c and 9-bc, and
366 Supp. Tables 1-4 (effect of coherence on the DV slopes, $p < 10^{-4}$). Nonetheless, we
367 formally tested the motor kinematics hypothesis by measuring the extent to which
368 neural activity during the stimulus viewing period predicts motor kinematic variables
369 in both tasks. Our analysis focused on movement onset time after the Go cue (reaction
370 time, RT) and hand velocity, both of which known to be reflected in the activity of
371 PMd and M1 neurons (Afshar et al., 2011, Kubota and Hamada, 1979, Churchland et
372 al., 2006a, Churchland et al., 2006b). We performed Ridge regression of both
373 kinematic variables onto population neural activity to determine the time when
374 kinematic signals appear in PMd and M1.
375
376 For the fixed duration task, our prediction of RT from neural population data was
377 poor in the targets and dots epochs as expected from the task design (Fig. 4 a-b). Only
378 late in the delay period (~last 50 ms), when the monkey was presumably planning the
379 arm movement, did we observe a very small rise in RT variance explained by neural
380 activity. This rise became significant for both areas and targets within 60 ms after the
381 go cue (Wilcoxon signed-rank test $p < 0.01$, Holm-Bonferroni correction for multiple
382 comparisons). We observed a wide range of RTs in both tasks, which lead to a strong
383 dynamic range in firing rates that correlated with RT after the go cue and thus lead to
384 high R^2 values, which are expected for (pre)motor brain regions. Crucially, the results
385 for the variable duration task were similar in terms of temporal profile, with
386 significant R^2 values only present after the go cue but not during dots (Fig. 4 c-d,
387 Supp. Figs 12 and 13 show model performance for example sessions). Repeating the
388 same analysis for hand peak velocity, we observed only modest R^2 values after the go
389 cue and around the time of the response for both tasks (Fig. 4 e-h). The absence of
390 significant R^2 values during the stimulus presentation period in our two tasks (Fig. 4
391 a-h) confirmed that hand motor signals were not contaminating our DV estimates.
392

393   Finally, and to rule out the contamination from additional variables associated with
394   the eye movement, we performed the same analyses on the analogous saccade
395   parameters: saccade RT and saccade peak velocity. Similar to our results for hand
396   movement kinematics, we could predict a significant fraction of variance of saccade
397   RT only during and following the go cue (but not before) (Supp. Fig. 14 a-d). The R^2
398   peaks for saccade RTs were significantly lower than those for hand RTs (Fig. 4 a-d vs
399   Supp. Fig. 14 a-d) (Wilcoxon signed-rank test for peak R^2 Hand vs Eye RT: p<5e-4
400   for all areas, tasks and target directions). Further, saccade peak velocity was not
401   explained by PMd or M1 neural data at any point in the trial (Supp. Fig. 14 e-h). The
402   weaker representation of eye kinematics after Go cue is consistent with the expected
403   role of PMd and M1 in controlling arm movements.
404
405   In summary, our results showed that regardless of task timing, motor parameter
406   representation in PMd and M1 was reliable only around and after the go cue and not
407   while the visual evidence was presented. Thus, the accelerated dynamics of choice
408   predictive activity early in the stimulus presentation period of the variable duration
409   task was not due to a contamination by motor signals.
410

Progressive recruitment of choice selective neurons underlies accelerated
dynamics of the DV in the variable duration task

413
414   In the previous sections, we showed that the dynamics of choice related neural
415   activity on single trials is flexible, being strongly influenced by the expected statistics
416   of stimulus duration. In conventional evidence integration models of decision
417   formation (Ratcliff and McKoon, 2007, Lo and Wang, 2006, Mazurek, 2003) changes
418   in the dynamics of the DV are implemented through parameters that govern the
419   accumulation of sensory evidence. We tested whether these models could replicate
420   our observation that the DV buildup rates are higher in the variable duration task, and
421   that the size of the increase is independent of motion coherence.
422
423   We focused on a simple formulation of integration-to-bound models, in which two
424   competing integrators accumulate noisy evidence about motion energy over time
425   toward a decision bound (Kiani et al., 2014a). As soon as one of the integrators
426   reaches the bound, a choice is made and the two integrators maintain their state
427   (integrated evidence) until the end of the trial (Kiani et al., 2008, Shadlen and
428   Newsome, 2001). We simulated two pools of spiking neurons whose mean firing rates
429   represent the state of integrators. Finally, we trained our logistic classifier on the spike
430   counts of the simulated neurons and calculated the DV buildup rates, just as we did
431   for our recorded neurons.
432
433   We envisioned three possible mechanisms for changes in the DV dynamics, each of
434   which can account for the observed psychophysical data with appropriate parameter
435   adjustments (Fig. 5a). The first two are based on known phenomena: urgency
436   (Churchland et al., 2008, Purcell and Kiani, 2016) and sensory gain (Cisek et al.,
437   2009). Urgency is an evidence-independent signal that drives both integrators toward
438   their bounds. In principle, an overall increase of urgency in the variable-duration task
439   might mimic a coherence-independent increase in the DV buildup rates as observed in
440   the physiological data (Fig. 3b,c, vertical shift in DV slope vs. coherence traces)
441   through faster commitment to choice. However, because urgency affects both
442   accumulators, and the DV depends largely on the *difference* in the activity of our two

443   pools of neurons, the effect of urgency on the DV slope is small unless very large
444   urgency signals are imposed (Fig. 5b, note that the cyan, red, and black data points are
445   almost completely superimposed in this figure). A large urgency signal is
446   mathematically equivalent to a reduction in the decision bound and would lead to less
447   accurate choices and, consequently, to a sizeable increase in psychophysical
448   thresholds in the variable duration task (Fig. 5c). Although the data of monkey F
449   provided some support for increased threshold, monkey H was incompatible with the
450   prediction of the urgency model (Supp. Fig. 15).

451

452   The sensory gain model builds on the proposal that later sensory evidence is
453   progressively amplified with a gain factor before integration (Cisek et al., 2009). The
454   original proposal by Cisek and colleagues assumes a leaky integration process with a
455   short time constant (Cisek et al., 2009) but in our tests the time constant of integration
456   was not a key factor. Similar to increased urgency, increased gain on sensory inputs
457   might lead to a coherence-independent increase in DV slope by accelerating bound
458   crossing and causing earlier commitment to choice. However, just as we showed for
459   the urgency signal, modest increases in gain do not generate a significant change in
460   the DV slopes as these largely depend on the difference between the accumulators,
461   both of which are affected by the increase in gain (Fig. 5b, red data points are largely
462   superimposed on cyan and black). While large gains can increase the DV slope, they
463   also lead to reduced performance accuracy (Fig. 5d) because the bound crossing is
464   accelerated and effective integration time is shortened, similar to what we observed
465   for the urgency signal above. The data from monkey H reduce the likelihood that the
466   urgency or sensory gain mechanisms are the only causes of the accelerated DVs in the
467   variable duration task.

468

469   Our third hypothesis proposes that the accelerated dynamics of the DV is due to
470   progressive recruitment of additional neural signals under conditions of temporal
471   uncertainty that represent choice outcome, which we term "categorical choice", but
472   not the accumulation of sensory evidence that leads to the choice. We postulate that
473   these categorical choice signals appear in each pool of accumulator neurons with
474   increasing frequency as each accumulator nears its bound (see below). In our
475   implementation, the strength of the categorical choice signal varies across single
476   neurons and is independent of the strength of the accumulated evidence signal in each
477   neuron (see Methods, γ_i values). In effect, the weighted contributions of these
478   neurons constitute a subspace of the neural population activity carrying coherence-
479   independent choice signals. This "categorical choice subspace" would not contribute
480   to the formation of the decision but might be necessary for translating the output of
481   the integration process into preparation for a specific operant action. Hereafter, for
482   brevity, we'll refer to this subspace as the "choice subspace".

483

484   In principle, this choice subspace could be encoded by a population of dedicated
485   neurons that transition from an uncommitted state (baseline firing rate) to a
486   committed state for choice 1 or choice 2, with the transition becoming more probable
487   as each accumulator approaches its decision bound. We, however, favor the
488   alternative implemented in our simulations—the same neurons that represent
489   integration of evidence also represent the categorical choice. This mixed selectivity at
490   the level of single neurons leads to the representation of choice and evidence
491   accumulation in separable subspaces at the level of population responses. These two
492   methods for implementation of the categorical choice signal have similar

10

493   consequences for the behavior and calculated DVs, but the latter is more in line with
494   previous observations in frontal cortex (Mante et al., 2013).
495
496   As suggested above, we simulated this mixed selectivity in a population of model
497   neurons whose responses were weighted sums of accumulated evidence and a
498   categorical choice signal (Methods, Integration Models). The choice signal was a
499   nonlinear monotonic function of the distance of the accumulated evidence from the
500   decision bound and can be thought of as a readout of the accumulation process in
501   preparation for commitment to a choice. We call this the progressive recruitment
502   model (PRM) for representation of choice signals. In the variable duration task,
503   acceleration of the choice signal enhances the representation of the upcoming choice
504   and boosts the model DV, leading to a coherence independent increase in DV slopes
505   (Fig. 5b, note that the magenta points are offset vertically from cyan, black and red).
506
507   PRM captures the behavioral data well because accelerated recruitment of coherence-
508   independent choice signals does not cause perturbations in the underlying integration
509   process and does not change psychophysical performance (Fig. 5a).   Thus the PRM
510   neatly captures the key behavioral (Fig. 5a) and physiological data (Fig. 5b) in
511   monkey H. In contrast to monkey H, psychophysical thresholds for monkey F
512   increased under conditions of temporal uncertainty, implying changes in the
513   underlying integration process (e.g., increased urgency or sensory gain).
514   Importantly, accelerated choice representation could happen simultaneously with
515   changes in the integration process that could cause an increased psychophysical
516   threshold for monkey F. Overall, our modeling results suggest that accelerated choice
517   representation, either in isolation or mixed with urgency or sensory gain, plays a key
518   role in enhanced response dynamics in PMd and M1 in the variable duration task.
519
520   **The progressive recruitment model makes specific predictions at the population**
521   **and single unit levels**
522
523   The PRM, as implemented in our simulations, makes specific, testable predictions
524   about the spatiotemporal features of the neural responses in both the fixed and
525   variable duration tasks. First, at the population level, the choice representing subspace
526   should be stable during a trial as more units are recruited to maintain a representation
527   of choice. Such stability facilitates decoding by downstream areas in the presence of
528   timing differences in our tasks. Second, this stabilization should happen faster in the
529   variable duration task due to the accelerated recruitment of choice representing
530   neurons. Third, the choice subspace in the population responses should be shared
531   across the two tasks. Fourth, at the single unit level we should observe the progressive
532   onset of choice representing units, some during the psychophysical integration
533   window (Fig.1d) and some only later in the trial. These units should have stable
534   choice preference (left or right) and stable or increasing choice modulation and their
535   recruitment should be accelerated in the variable duration task.
536
537   For simplicity in our simulations, we assumed no categorical choice representation in
538   the fixed duration task (Methods, Integration Models). Similar results would have
539   been obtained, however, if categorical choice signals were also recruited in this task
540   (a non-zero average γ_i parameter) as long as they remained substantially lower than in
541   the variable duration task. We expect this to be a more plausible scenario, and the
542   extent to which progressive recruitment is present in the fixed duration task can be

11

543   tested empirically.

544

545   In the following two sections we test these predictions first at the population level and
546   then at the single unit level.

547

548   **Choice signal stabilizes during stimulus presentation in PMd and M1**

549

550   To test our predictions, we started by examining the structure of the temporal
551   representation of choice across the entire trial. For each time point in each task we
552   defined a "choice axis" that best represents modulation of neural responses with
553   choice. Neurons with strong choice modulation at that time had a large weight in the
554   choice axis and neurons with smaller modulation had smaller weights (see Methods).
555   By comparing the similarity of choice axes at different times and in different tasks,
556   we could quantify the stability of choice-representation in the population. Fig. 6
557   shows the inner product of choice axes at different times. A large inner product
558   suggests good alignment of the choice axes and high stability of the choice-
559   representing subspace. Conversely, a low inner product suggests a rotation in the
560   choice axis, which could happen if two different sub-populations of neurons represent
561   the choice at different times or if the relative contribution of neurons to the
562   representation of choice changes over time. Mathematically, the projection of a choice
563   axis on itself would be 1, making the diagonals uninformative. We therefore
564   calculated two choice axes for each point in time for two independent halves of each
565   session's data and measured the projection of these two axes onto each other (see
566   Methods). This way, the diagonal elements of the projection matrix were not set to 1
567   but instead provided a measure of self-consistency of the choice axis. Armed with
568   these stability and self-consistency metrics we investigated our model predictions.

569

570   Starting with PMd in the fixed duration task (Fig. 6a, Supp. Figs 16a and 17a), we
571   observed three important features. First there was a gradual emergence, rotation and
572   stabilization of the choice axis (emergence of square structure in the heat map) that
573   started ~350 ms after dots onset and unfolded over the remainder of the dots
574   presentation. Second, the dots period was followed by a highly stable choice signal in
575   the delay period. Importantly, the choice axes late in the dots period were largely
576   overlapping with the choice axes early in the delay period (up until the go cue)
577   indicating that the representation of choice was largely maintained even in the
578   absence of additional visual evidence. Third, the choice signal around the initiation of
579   the reach, despite being extremely strong, was also very transient in its direction in
580   neural state space. These three main features were recapitulated for M1 (Fig. 6b,
581   Supp. Figs 16b and 17b), the main difference being the latency for stabilization of the
582   choice axis during the dots presentation, which happened faster for PMd (~350ms
583   after dots onset) compared to M1 (>500 ms after dots onset). The temporal ordering
584   between the two areas was consistent with our earlier analysis of choice predictive
585   activity in the fixed duration task (Fig. 2a). These results are consistent with the first
586   prediction from the PRM regarding stability of the choice subspace during dots and
587   delay period.

588

589   For the variable duration task the rotation and stabilization of the choice axis
590   happened much faster (~250 ms after dots onset) than in the fixed duration task,
591   consistent with the second prediction of PRM. In the variable duration task, in fact,
592   the temporal stabilization of the choice axis was virtually indistinguishable between

12

593   PMd and M1 (Fig. 6c-d, Supp. Figs 16c-d and 17c-d).

594

595   The heat maps provide a qualitative description of stability of the choice subspace.
596   We quantified stability *within* and *across* epochs using decoding analyses (see
597   Methods). Our results show substantial choice representation stability within the
598   target, dots and pre-go epochs, but not the peri-movement epoch (Supp. Fig. 18 and
599   19). In addition, our results demonstrate choice representation stability across the dots
600   and pre-go epochs but not across other pairs of epochs (Supp. Fig. 20).

601

602   Finally, our results also suggest a stable choice representation across tasks. Taking
603   advantage of sessions in which we recorded the same units in each brain area while
604   the monkey performed both tasks, we compared alignment of choice axes across time
605   and tasks (Fig. 6e-f). The choice axis measured in the stimulus presentation for the
606   variable duration task was largely consistent with choice axes at later times in the
607   fixed duration task (and vice versa), in agreement with the third prediction of the
608   PRM. This implies that the same transformation from integration of evidence to
609   stable choice signal occurs in the two tasks and is being carried out through the
610   recruitment of the same units, only at different rates that reflect the cognitive demands
611   imposed on the subject.

612

613   **Stabilization of population choice axes occurs through progressive recruitment**
614   **of neurons with sustained choice modulation**

615

616   We next examined the choice modulation at the single unit level to test the fourth
617   prediction of the PRM. This analysis provides a bridge between our population
618   analyses, modeling results, and single unit properties. We first calculated the
619   cumulative fraction of units that display significant choice modulation as stimulus
620   presentation progresses. Consistent with the PRM, the cumulative fraction rises much
621   faster over the course of stimulus presentation in the variable duration task (dashed
622   lines) compared to the fixed duration task (solid lines) for both PMd (Fig. 7a, Supp.
623   Fig. 21a and 22a) and M1 (Fig. 7b, Supp. Fig. 21b and 22b).

624

625   Further support for a mechanism of progressive recruitment came from persistent
626   activity of choice-selective neurons. We used area under the ROC (Shadlen and
627   Newsome, 2001) (auROC) to quantify how well single neuron responses represented
628   choice at each time point during the trial. If the representation of choice at the single
629   neuron level is stable over time, a heat map of auROC of individual neurons, ordered
630   by onset of choice representation, should show an upper triangular structure. In
631   contrast, transient representation of choice in individual neurons should be evident as
632   a diagonal structure in the heat map (Harvey et al., 2012, Morcos and Harvey, 2016).
633   Fig. 7c-d showed a strong upper triangular structure for units with significant choice
634   modulation (above the gray dashed line), indicating persistent choice modulation over
635   the course of the trial. The existence of units that only become choice modulated late
636   in the dots period or even during the delay period for both PMd (Fig. 7c) and M1 (Fig.
637   7d) matches our expectation that progressive recruitment of choice signals is also
638   present in the fixed duration task.

639

640   Consistent with our logistic regression results, the emergence of persistent choice
641   representation in the individual units was faster and more widespread in PMd (Fig. 7c
642   Supp. Fig. 23a) than M1 (Fig. 7d, Supp. Fig. 24b) in the fixed duration task.

643
644 For a direct comparison across areas and tasks we also calculated the area under ROC
645 traces for sessions in which fixed and variable duration tasks were run in the same
646 experimental session (while putatively recording from the same units, see Methods).
647 The results show that for both areas (Fig. 7e-f, Supp. Fig. 24c-d), units with stable
648 modulation were recruited earlier during the trial, and just as in the fixed duration
649 task, maintained their modulation strength until close to the time of the arm
650 movement. Not only did the same units represent choice in both areas during the
651 stimulus presentation period (Fig. 6e-f), but also their recruitment ordering was
652 consistent across tasks for both areas (Spearman correlation between latencies across
653 tasks for PMD: rho = 0.869, p = 1.37×10^{-11} and M1: rho = 0.579, p = 3.79×10^{-5} for the
654 example session shown in Fig. 7e-f), further suggesting that the same transformation
655 of signals is happening in both tasks at different rates. Finally, for the variable
656 duration task, just as in the logistic regression analysis (Fig. 3a), the differences
657 between the two areas largely vanished in the variable duration task, both in terms of
658 fraction of significant units and rate of recruitment. Taken together these results
659 corroborate the fourth prediction from the PRM and show that temporal stability of
660 choice predictive signals inferred at the population mechanism is present at the level
661 of individual units as well.
662
663
664 **Choice signal is distributed across the neural population**
665
666 The stability of the choice axis over time (Figs. 6,7) suggests that there is little relay
667 of information between different ensembles of neurons (sequence mechanism:
668 (Harvey et al., 2012, Morcos and Harvey, 2016, Rajan et al., 2016, Scott et al., 2017))
669 once the choice signal appears in the PMd and M1 populations. To further test
670 whether a sequence mechanism might be compatible with our results, we quantified
671 the distribution of choice-related neurons in the population as a function of time
672 during the trial. If the choice representation is generated by a sequence mechanism,
673 the neural representations at a given time during the trial should critically depend on a
674 small number of key neurons. Removing these neurons from the population should
675 result in a drastic degradation in the quality of the neural representations (Haxby et
676 al., 2001, Kiani et al., 2007). We tested this possibility by performing a unit dropping
677 analysis that calculates how prediction accuracy is impacted by exclusion of the best
678 units (Kiani et al., 2015).
679
680 We illustrate our results by focusing on two points in time: the end of the stimulus
681 presentation period (last 50 ms) and go cue presentation (50 ms before go), because a
682 strong choice related signal is present at these times in both tasks. Our results (Fig. 8a,
683 Supp. Fig. 24a and 25a) show that predictive accuracy decayed smoothly as the best
684 units were removed for both areas and both monkeys. We did not observe any
685 precipitous drop in prediction accuracy that might suggest a special role for a small
686 group of transiently active neurons. PMd remained more predictive than M1 at the
687 end of stimulus presentation (Fig. 8a, Supp. Fig. 24a and 25a), as expected from
688 previous sections of this paper. This discrepancy vanished around the go cue. Also, in
689 the variable duration task the decay in performance was shallower (up to only ~10%
690 for the best 70 units) compared to the fixed duration task (Fig. 8b, Supp. Fig. 24b and
691 25b) due to the higher number of strongly tuned units (Fig. 7). The key observation is
692 that representations in both areas and in both time points show remarkable robustness

14

693   to exclusion of the best predictive single units. Even after dropping 70 best units
694   (corresponding to a median 46%/33% of units in PMd and 48%/31% of units in M1 in
695   the fixed/variable duration tasks respectively) choice prediction accuracies remained
696   well above chance.
697
698

699   **Discussion**

700
701   The primary goals of this study were: 1) investigate whether single-trial, decision-
702   related activity in PMd and M1 has the properties of a DV and determine whether and
703   how DV dynamics depend on uncertainty about stimulus timing, 2) test computational
704   models to identify mechanisms that can explain the observed choice behavior and
705   neural dynamics, and 3) examine the spatio-temporal features of decision-related
706   signals, under conditions of both temporal certainty and uncertainty, with a specific
707   goal of differentiating between stable vs. sequential representations of choice-
708   predictive signals. To achieve these goals we employed two variants of a classical
709   motion discrimination task, fixed and variable duration (Kiani et al., 2008, Shadlen
710   and Newsome, 2001), and combined them with multi-electrode recordings and
711   decoding techniques to obtain reliable single trial estimates of decision-related
712   dynamics at the level of the neural population.

713
714   **Population neural activity in PMd and M1 exhibit properties of a decision**
715   **variable.**

716
717   Our neural population data are consistent with predictions of classic accumulation-to-
718   bound models of the decision process. Specifically, choice predictive activity emerges
719   quickly after stimulus onset in both PMd and M1 and increases with time and
720   stimulus coherence as expected from evidence accumulation (integration) linked to
721   the sensory stimulus. Critically, our simultaneous population recordings provided
722   statistical power to test these predictions on single-trial activity as opposed to trial-
723   averaged activity as in most previous studies. The build-up of choice predictive
724   activity on single trials—as captured in the rate-of-rise of the logistic decision
725   variable—varied systematically with stimulus coherence (Figs. 2d,e, 3b,c; Suppl.
726   Tables 1-3) as expected from accumulator models (Shadlen and Newsome, 2001,
727   Roitman and Shadlen, 2002, Bollimunta et al., 2012) and inconsistent with step like
728   transitions in the neural states (Latimer et al., 2015, Miller and Katz, 2010).

729
730   Choice-predictive activity was present in both PMd and M1 even when action
731   initiation was cued more than one second after termination of the visual stimulus. The
732   most pronounced difference between the two areas occurred in the fixed duration
733   task: significant choice related activity emerged faster and was stronger in PMd
734   compared to M1 (Fig. 2b,c). These differences are consistent with the standard view
735   of a greater cognitive role for PMd compared to M1 (Cisek and Kalaska, 2005,
736   Coallier et al., 2015, Wise et al., 1997), and with the idea of a rostro-caudal gradient
737   of visuomotor responses in PMd/M1 (Cisek and Kalaska, 2005) with stronger motor
738   signals in caudal PMd/M1 and stronger target selection signals in pre-PMd/ rostral
739   PMd.

740
741   This difference, however, essentially vanished in the variable duration task. Following
742   stimulus onset, prediction accuracy increased at nearly identical rates in the two areas

743 and plateaued at similarly high levels, the only difference being ~20 msec longer
744 latencies in M1 (Fig. 3a). The dynamics accelerated in both areas under conditions of
745 temporal uncertainty, but the change was particularly dramatic in M1 (compare Fig.
746 2a with Fig. 3a). These results could not be explained by displacement of motor
747 kinematic signals into the stimulus presentation period in the variable duration task
748 (Fig. 4). Importantly, the accelerated dynamics were independent of the coherence of
749 the visual stimulus; the DV slope vs. coherence curves for the variable duration
750 condition are essentially vertically offset copies of those for the fixed duration
751 condition.
752
753 To our knowledge only one other study (Shadlen and Newsome, 2001) employed both
754 fixed and variable duration motion discrimination tasks while recording decision-
755 related activity in individual units. Similar to the current study, the authors observed a
756 larger and faster average increase in choice modulation in LIP neurons in the variable
757 duration task, which they speculated could reflect increased urgency to make quicker
758 decisions when the duration of the sensory evidence is uncertain. While this intuition
759 is appealing, it begs the question as to the actual mechanism underlying the
760 accelerated dynamics, which we explored through a series of quantitative models.
761
762 **Progressive recruitment of choice-selective neurons**
763
764 The discovery of single-trial, coherence-independent acceleration of DV dynamics
765 under conditions of temporal uncertainty provides a useful new constraint on
766 mechanistic models of the decision process. Different variants of race models
767 between accumulation processes have long been proposed to explain both behavior
768 (Beck et al., 2008, Link, 1992, Vickers, 1970, Wong and Wang, 2006) and neural
769 activity in premotor structures (Churchland et al., 2008, Hanks et al., 2014, Scott et
770 al., 2017) during perceptual decision tasks. In this study we implemented three
771 variants of race models that attempted to explain both the observed psychophysical
772 behavior and the single trial DV dynamics across both tasks. The increased gain and
773 increased urgency models could not replicate the DV dynamics for the variable
774 duration task without unacceptable deterioration in psychophysical performance. In
775 contrast, our novel progressive recruitment model (PRM) with an adaptable
776 recruitment rate closely matched both the physiological and behavioral data. This
777 model proposes that PMd and M1 population activity reflect recruitment of a second,
778 coherence-independent "choice" signal in addition to the well-known coherence-
779 dependent signal. Importantly, the PRM and accumulation-to-bound models are not
780 incompatible. PRM simply adds a twist to how choice is represented while evidence
781 accumulation proceeds during a trial.
782
783 **Temporal stability and latency of choice representation in PMd and M1**
784
785 The analyses of choice axes suggested a stable representation of choice during the
786 dots and delay period. However, we found that the choice axis early in the dots period
787 (~250 ms after dots onset) does not perfectly overlap with choice axis late in the dots
788 period (~750 ms after dots onset). Through our simulations, we posited that changes
789 in the choice axis between the early and late epochs of the dots period occur due to
790 the recruitment of signals associated with the categorical choice in addition to signals
791 associated with the accumulation of evidence. Similarly, but to a much larger degree,
792 the choice axis during the actual arm movement did not overlap with the choice axis

16

793 from the dots period, probably reflecting the additional recruitment of signals
794 associated with moving the arm. We believe that the shift in the choice axis across
795 epochs is evidence for the existence of multiple choice subspaces in PMd/M1 (and
796 other brain regions) that are engaged at different epochs in the tasks presented here
797 (and for other tasks). In this study, we have exposed one aspect of these choice
798 subspaces. Multiple choice subspaces will likely reflect the different behavioral
799 demands for the monkey at different points in the task such as sensory evidence
800 evaluation, motor preparation, movement execution, post-movement evaluation,
801 reward expectation, and learning. Reorganization of neural activity into different
802 subspaces has been previously observed in PMd for delayed reach tasks between the
803 movement preparation and execution phases (Elsayed et al., 2016) and is compatible
804 with the low projection between peri-movement and delay period axes we obtained in
805 the fixed duration task (Figure 6a).

807 We also observed a difference in latency for choice representation to become stable
808 between PMd and M1, and these latency differences depended on the task. For the
809 variable duration task, the latencies for stabilization of the choice representation in
810 both PMd and M1 were well within the estimated psychophysical integration
811 windows for both monkeys (500-600 msec—Fig. 1d). In contrast, M1 data in the
812 fixed duration task appear to stabilize at ~750 msec (Fig. 6b), well outside the
813 psychophysical integration window. Thus, the M1 delay can be highly variable
814 depending on the expected time for the execution of motor action. In the variable-
815 duration task, where the Go cue can happen any time, M1 responses reflect the choice
816 much earlier. Note that similar progressive recruitment of the choice representing
817 subspace in M1 and PMd would lead to similar reduction of latency in the two areas.
818 Therefore, it is unlikely that a common input to the two areas underlies our results.
819 An appealing hypothesis is that changes of latency in M1 are caused by changes of
820 PMd dynamics. If the choice representation in PMd should reach a threshold level
821 before it emerges in M1, the accelerated choice representation in PMd would cause
822 both accelerated dynamics and significantly reduced latency of choice representation
823 in M1 in the variable duration task. Overall, our results hint at a mechanism where
824 PMd responses lead and furnish the choice representation in M1.

827 **Progressive recruitment accounts better for our data than a sequence hypothesis**

829 Our results suggest that progressive recruitment of units with temporally stable choice
830 modulation is a plausible mechanism for choice representation in PMd and M1. In
831 contrast, evidence from recent optical imaging studies in rodents (Harvey et al., 2012,
832 Morcos and Harvey, 2016) suggests an alternative mechanism: representation of
833 choice by transient ensembles of neurons that are activated sequentially as the trial
834 proceeds, effectively passing choice information from one ensemble to the next
835 throughout a trial. Intrigued by this finding in rodents, we analyzed our neural
836 population data to test the predictions of these two mechanisms on individual sessions
837 in monkeys. Our analyses of the temporal stability of choice axes, within and across
838 epoch decoding, and unit dropping all support a stable choice representation
839 mechanism over a sequence mechanism. Our failure to detect sequences during the
840 visual stimulus and delay periods does not reflect a problem with our analysis
841 techniques; sequences of ensemble activity were strikingly present in the peri-
842 movement interval for the operant arm movement, as shown by the diagonal structure

17

843 in the lower right portion of each plot in Figure 6. This diagonal structure results from
844 fast modulations around movement onset that are expected because of impending
845 changes in limb position and kinematics during movement, as reported before
846 (Churchland et al., 2010, Churchland et al., 2012). At the individual unit level our
847 results also matched the progressive recruitment model predictions: the choice signal
848 is carried by a large (and growing) fraction of neurons (Fig. 7a,b) and their
849 modulation is largely stable over the stimulus presentation and pre-go cue period
850 (ROC analyses, Fig. 7c,d).
851
852 The pronounced difference between stable choice representation in the primate cortex
853 and sequential representation in the rodent cortex might simply reflect a species
854 difference in neural mechanisms underlying choice behavior. However, a recent
855 study of choice mechanisms in rodents supports stable accumulation of evidence in
856 parietal cortex (Hanks et al., 2015). The key difference between the latter study and
857 those that yielded evidence for sequences is that animals were actively locomoting on
858 a track ball when sequences were observed. A more recent—and as yet not peer
859 reviewed—study suggests that sequences of neuronal activity during track ball
860 locomotion result not from choice-related signals per se, but from specific
861 combinations of bodily position and head angle at successive times during locomotion
862 (Krumin et al., 2017). Our best reading of the current literature is that the evidence for
863 stable representations of choice in primate cortex is strong, whereas the sequence
864 hypothesis that has emerged from rodent work requires further study to confirm,
865 refine, or reject. Developing behavioral tasks that are as similar as possible for
866 monkeys and rodents may help resolve some of these issues.
867
868 **Concluding remarks**
869
870 We have focused on single trial estimation of decision variables in neural population
871 data and development of mechanistic models that explain both the behavioral and
872 physiological data. Like many studies in the contemporary literature, our comparison
873 of models to data relies on regression analyses that produce vectors of weights on the
874 responses of individual units, be they neurons or voxels. Importantly, we do not
875 assert that a downstream brain area or deeper cortical layer (Chandrasekaran et al.,
876 2017) actually performs a linear weighting of PMd/M1 activity in superficial layers to
877 guide decisions. For present purposes, we simply use the DV as a proxy for the
878 informational content about choice present at any given moment in these neural
879 populations (Kiani et al., 2014b). Recordings across multiple brain regions and
880 precise knowledge of projection pathways between them will be required to elucidate
881 the actual mechanisms that transform this information to signals that trigger an action.
882
883 More broadly, our study integrates a small but growing body of literature that
884 leverages simultaneous electrophysiological population recordings to explore the
885 neural substrate of internal cognitive phenomena at the level of single trials
886 (Bollimunta et al., 2012, Kaufman et al., 2015, Kiani et al., 2014b, Rich and Wallis,
887 2016). This approach promises to shed light on internal cognitive processes whose
888 dynamics vary substantially from trial to trial (e.g. decision-making, attention). In the
889 future, the strengths of this approach will be amplified by monitoring
890 cognitive/attentional states in real time and probing the subject and circuit in a
891 neurally contingent manner.
892

Acknowledgments

Author Contributions

All authors contributed extensively to the conceptualization of the study, the experimental design and choice of methods for data analysis. D.P. trained animals, performed all electrophysiological experiments, collected and analyzed data. D.P., R.K. and W.T.N. wrote initial draft of the paper. S.I.R, D.P and R.K. performed the surgical procedures. All authors contributed analytical insights and commented on statistical tests, discussed the results and implications, and contributed extensively to the multiple subsequent drafts of the paper.

Declaration of Interests

The authors declare no competing interests.

References

AFSHAR, A., SANTHANAM, G., YU, BYRON M., RYU, STEPHEN I., SAHANI, M. & SHENOY, KRISHNA V. 2011. Single-Trial Neural Correlates of Arm Movement Preparation. *Neuron,* 71**,** 555-564.

BECK, J. M., MA, W. J., KIANI, R., HANKS, T., CHURCHLAND, A. K., ROITMAN, J., SHADLEN, M. N., LATHAM, P. E. & POUGET, A. 2008. Probabilistic Population Codes for Bayesian Decision Making. *Neuron,* 60**,** 1142-1152.

BOLLIMUNTA, A., TOTTEN, D. & DITTERICH, J. 2012. Neural Dynamics of Choice: Single-Trial Analysis of Decision-Related Activity in Parietal Cortex. *The Journal of Neuroscience,* 32**,** 12684.

941   BRITTEN, K. H., NEWSOME, W. T., SHADLEN, M. N., CELEBRINI, S. & MOVSHON, J.
942   A. 1996. A relationship between behavioral choice and the visual
943   responses of neurons in macaque MT. *Visual Neuroscience,* 13**,** 87-100.
944   BRITTEN, K. H., SHADLEN, M. N., NEWSOME, W. T. & MOVSHON, J. A. 1992. The
945   analysis of visual motion: a comparison of neuronal and psychophysical
946   performance. *J. Neurosci.,* 12**,** 4745-4765.
947   BRODY, C. D. & HANKS, T. D. 2016. Neural underpinnings of the evidence
948   accumulator. *Curr Opin Neurobiol*.
949   CELEBRINI, S. & NEWSOME, W. T. 1994. Neuronal and psychophysical sensitivity
950   to motion signals in extrastriate area MST of the macaque monkey. *The
951   Journal of Neuroscience,* 14**,** 4109.
952   CHANDRASEKARAN, C., PEIXOTO, D., NEWSOME, W. T. & SHENOY, K. V. 2017.
953   Laminar differences in decision-related neural activity in dorsal premotor
954   cortex. *Nature Communications,* 8**,** 614.
955   CHURCHLAND, A. K., KIANI, R. & SHADLEN, M. N. 2008. Decision-making with
956   multiple alternatives. 11**,** 693-703.
957   CHURCHLAND, M. M., AFSHAR, A. & SHENOY, K. V. 2006a. A Central Source of
958   Movement Variability. *Neuron,* 52**,** 1085-1096.
959   CHURCHLAND, M. M., CUNNINGHAM, J. P., KAUFMAN, M. T., FOSTER, J. D.,
960   NUYUJUKIAN, P., RYU, S. I. & SHENOY, K. V. 2012. Neural population
961   dynamics during reaching. *Nature,* 487**,** 51.
962   CHURCHLAND, M. M., CUNNINGHAM, J. P., KAUFMAN, M. T., RYU, S. I. & SHENOY,
963   K. V. 2010. Cortical Preparatory Activity: Representation of Movement or
964   First Cog in a Dynamical Machine? *Neuron,* 68**,** 387-400.
965   CHURCHLAND, M. M., SANTHANAM, G. & SHENOY, K. V. 2006b. Preparatory
966   Activity in Premotor and Motor Cortex Reflects the Speed of the
967   Upcoming Reach. *Journal of Neurophysiology,* 96**,** 3130-3146.
968   CISEK, P. 2007. Cortical mechanisms of action selection: the affordance
969   competition hypothesis. *Philos Trans R Soc Lond B Biol Sci,* 362**,** 1585-99.
970   CISEK, P. 2012. Making decisions through a distributed consensus. *Curr Opin
971   Neurobiol,* 22**,** 927-36.
972   CISEK, P. & KALASKA, J. F. 2005. Neural correlates of reaching decisions in dorsal
973   premotor cortex: specification of multiple direction choices and final
974   selection of action. *Neuron,* 45**,** 801-14.
975   CISEK, P. & KALASKA, J. F. 2010. Neural mechanisms for interacting with a world
976   full of action choices. *Annu Rev Neurosci,* 33**,** 269-98.
977   CISEK, P., PUSKAS, G. A. & EL-MURR, S. 2009. Decisions in Changing Conditions:
978   The Urgency-Gating Model. *The Journal of Neuroscience,* 29**,** 11560.
979   COALLIER, E., MICHELET, T. & KALASKA, J. F. 2015. Dorsal premotor cortex:
980   neural correlates of reach target decisions based on a color-location
981   matching rule and conflicting sensory evidence. *J Neurophysiol,* 113**,**
982   3543-73.
983   DE LAFUENTE, V., JAZAYERI, M. & SHADLEN, M. N. 2015. Representation of
984   accumulating evidence for a decision in two parietal areas. *J Neurosci,* 35**,**
985   4306-18.
986   ELSAYED, G. F., LARA, A. H., KAUFMAN, M. T., CHURCHLAND, M. M. &
987   CUNNINGHAM, J. P. 2016. Reorganization between preparatory and
988   movement population responses in motor cortex. *Nature
989   Communications,* 7**,** 13239.

990 GOLD, J. I. & SHADLEN, M. N. 2007. The neural basis of decision making. *Annual*
991   *review of neuroscience,* 30**,** 535-74.
992 GOLDMAN-RAKIC, P. S. 1995. Cellular basis of working memory. *Neuron,* 14**,** 477-
993   485.
994 GUO, ZENGCAI V., LI, N., HUBER, D., OPHIR, E., GUTNISKY, D., TING,
995   JONATHAN T., FENG, G. & SVOBODA, K. 2014. Flow of Cortical Activity
996   Underlying a Tactile Decision in Mice. *Neuron,* 81**,** 179-194.
997 HANKS, T., KIANI, R. & SHADLEN, M. N. 2014. A neural mechanism of speed-
998   accuracy tradeoff in macaque area LIP. *eLife,* 3**,** e02260.
999 HANKS, T. D., KOPEC, C. D., BRUNTON, B. W., DUAN, C. A., ERLICH, J. C. & BRODY,
1000   C. D. 2015. Distinct relationships of parietal and prefrontal cortices to
1001   evidence accumulation. *Nature,* 520**,** 220-3.
1002 HANKS, T. D. & SUMMERFIELD, C. 2017. Perceptual Decision Making in Rodents,
1003   Monkeys, and Humans. *Neuron,* 93**,** 15-31.
1004 HARVEY, C. D., COEN, P. & TANK, D. W. 2012. Choice-specific sequences in
1005   parietal cortex during a virtual-navigation decision task. *Nature,* 484**,** 62-
1006   8.
1007 HAXBY, J. V., GOBBINI, M. I., FUREY, M. L., ISHAI, A., SCHOUTEN, J. L. & PIETRINI,
1008   P. 2001. Distributed and Overlapping Representations of Faces and
1009   Objects in Ventral Temporal Cortex. *Science,* 293**,** 2425.
1010 HEITZ, RICHARD P. & SCHALL, JEFFREY D. 2012. Neural Mechanisms of Speed-
1011   Accuracy Tradeoff. *Neuron,* 76**,** 616-628.
1012 HOSHI, E. 2013. Cortico-basal ganglia networks subserving goal-directed
1013   behavior mediated by conditional visuo-goal association. *Front Neural*
1014   *Circuits,* 7**,** 158.
1015 KAUFMAN, M. T., CHURCHLAND, M. M., RYU, S. I. & SHENOY, K. V. 2015.
1016   Vacillation, indecision and hesitation in moment-by-moment decoding of
1017   monkey motor cortex. *Elife,* 4**,** e04677.
1018 KIANI, R., CORTHELL, L. & SHADLEN, M. N. 2014a. Choice Certainty Is Informed
1019   by Both Evidence and Decision Time. *Neuron,* 84**,** 1329-1342.
1020 KIANI, R., CUEVA, C. J., REPPAS, J. B. & NEWSOME, W. T. 2014b. Dynamics of
1021   neural population responses in prefrontal cortex indicate changes of mind
1022   on single trials. *Curr Biol,* 24**,** 1542-7.
1023 KIANI, R., CUEVA, CHRISTOPHER J., REPPAS, JOHN B., PEIXOTO, D., RYU,
1024   STEPHEN I. & NEWSOME, WILLIAM T. 2015. Natural Grouping of Neural
1025   Responses Reveals Spatially Segregated Clusters in Prearcuate Cortex.
1026   *Neuron,* 85**,** 1359-1373.
1027 KIANI, R., ESTEKY, H., MIRPOUR, K. & TANAKA, K. 2007. Object Category
1028   Structure in Response Patterns of Neuronal Population in Monkey
1029   Inferior Temporal Cortex. *Journal of neurophysiology,* 97**,** 4296-4309.
1030 KIANI, R., HANKS, T. D. & SHADLEN, M. N. 2008. Bounded integration in parietal
1031   cortex underlies decisions even when viewing duration is dictated by the
1032   environment. *J Neurosci,* 28**,** 3017-29.
1033 KIANI, R. & SHADLEN, M. N. 2009. Representation of confidence associated with
1034   a decision by neurons in the parietal cortex. *Science (New York, N.Y.),* 324**,**
1035   759-764.
1036 KRUMIN, M., HARRIS, K. D. & CARANDINI, M. 2017. Decision and navigation in
1037   mouse parietal cortex. *bioRxiv*.

1038 KUBOTA, K. & HAMADA, I. 1979. Preparatory activity of monkey pyramidal tract
1039 neurons related to quick movement onset during visual tracking
1040 performance. *Brain Research,* 168**,** 435-439.
1041 KURATA, K. & HOFFMAN, D. S. 1994. Differential effects of muscimol
1042 microinjection into dorsal and ventral aspects of the premotor cortex of
1043 monkeys. *J Neurophysiol,* 71**,** 1151-64.
1044 LATIMER, K. W., YATES, J. L., MEISTER, M. L. R., HUK, A. C. & PILLOW, J. W. 2015.
1045 Single-trial spike trains in parietal cortex reveal discrete steps during
1046 decision-making. *Science,* 349**,** 184.
1047 LINK, S. W. 1992. *The wave theory of difference and similarity,* Hillsdale, NJ, US,
1048 Lawrence Erlbaum Associates, Inc.
1049 LO, C.-C. & WANG, X.-J. 2006. Cortico-basal ganglia circuit mechanism for a
1050 decision threshold in reaction time tasks. *Nat Neurosci,* 9**,** 956-963.
1051 MACHENS, C. K., ROMO, R. & BRODY, C. D. 2010. Functional, But Not Anatomical,
1052 Separation of "What" and "When" in Prefrontal Cortex. *The Journal of*
1053 *Neuroscience,* 30**,** 350.
1054 MANTE, V., SUSSILLO, D., SHENOY, K. V. & NEWSOME, W. T. 2013. Context-
1055 dependent computation by recurrent dynamics in prefrontal cortex.
1056 *Nature,* 503**,** 78-84.
1057 MAZUREK, M. E. 2003. A Role for Neural Integrators in Perceptual Decision
1058 Making. *Cerebral Cortex,* 13**,** 1257-1269.
1059 MEISTER, M. L., HENNIG, J. A. & HUK, A. C. 2013. Signal multiplexing and single-
1060 neuron computations in lateral intraparietal area during decision-making.
1061 *J Neurosci,* 33**,** 2254-67.
1062 MILLER, P. & KATZ, D. B. 2010. Stochastic Transitions between Neural States in
1063 Taste Processing and Decision-Making. *The Journal of Neuroscience,* 30**,**
1064 2559.
1065 MORCOS, A. S. & HARVEY, C. D. 2016. History-dependent variability in population
1066 dynamics during evidence accumulation in cortex. *Nature Neuroscience.*
1067 MURAKAMI, M. & MAINEN, Z. F. 2015. Preparing and selecting actions with
1068 neural populations: toward cortical circuit mechanisms. *Curr Opin*
1069 *Neurobiol,* 33**,** 40-6.
1070 MURPHY, P. R., BOONSTRA, E. & NIEUWENHUIS, S. 2016. Global gain modulation
1071 generates time-dependent urgency during perceptual choice in humans.
1072 *Nat Commun,* 7**,** 13526.
1073 PALMER, J., HUK, A. C. & SHADLEN, M. N. 2005. The effect of stimulus strength on
1074 the speed and accuracy of a perceptual decision. *J Vis,* 5**,** 376-404.
1075 PASSINGHAM, R. E. 1985. Premotor cortex: sensory cues and movement. *Behav*
1076 *Brain Res,* 18**,** 175-85.
1077 PESARAN, B., NELSON, M. J. & ANDERSEN, R. A. 2006. Dorsal Premotor Neurons
1078 Encode the Relative Position of the Hand, Eye, and Goal during Reach
1079 Planning. *Neuron,* 51**,** 125-134.
1080 PONCE-ALVAREZ, A., NÁCHER, V., LUNA, R., RIEHLE, A. & ROMO, R. 2012.
1081 Dynamics of Cortical Neuronal Ensembles Transit from Decision Making
1082 to Storage for Later Report. *The Journal of Neuroscience,* 32**,** 11956.
1083 PURCELL, BRADEN A. & KIANI, R. 2016. Neural Mechanisms of Post-error
1084 Adjustments of Decision Policy in Parietal Cortex. *Neuron,* 89**,** 658-671.

RAJAN, K., HARVEY, CHRISTOPHER D. & TANK, DAVID W. 2016. Recurrent Network Models of Sequence Generation and Memory. *Neuron,* 90**,** 128-142.

RAPOSO, D., KAUFMAN, M. T. & CHURCHLAND, A. K. 2014. A category-free neural population supports evolving demands during decision-making. *Nat Neurosci,* 17**,** 1784-92.

RATCLIFF, R. & MCKOON, G. 2007. The Diffusion Decision Model: Theory and Data for Two-Choice Decision Tasks. *Neural Computation,* 20**,** 873-922.

RICH, E. L. & WALLIS, J. D. 2016. Decoding subjective decisions from orbitofrontal cortex. *Nat Neurosci,* 19**,** 973-80.

ROITMAN, J. D. & SHADLEN, M. N. 2002. Response of neurons in the lateral intraparietal area during a combined visual discrimination reaction time task. *J Neurosci,* 22**,** 9475-89.

SASAKI, K. & GEMBA, H. 1986. Effects of premotor cortex cooling upon visually initiated hand movements in the monkey. *Brain Res,* 374**,** 278-86.

SCOTT, B. B., CONSTANTINOPLE, C. M., AKRAMI, A., HANKS, T. D., BRODY, C. D. & TANK, D. W. 2017. Fronto-parietal Cortical Circuits Encode Accumulated Evidence with a Diversity of Timescales. *Neuron,* 95**,** 385-398.e5.

SHADLEN, M. N. & KIANI, R. 2013. Decision making as a window on cognition. *Neuron,* 80**,** 791-806.

SHADLEN, M. N., KIANI, R., NEWSOME, W. T., GOLD, J. I., WOLPERT, D. M., ZYLBERBERG, A., DITTERICH, J., DE LAFUENTE, V., YANG, T. & ROITMAN, J. 2016. Comment on "Single-trial spike trains in parietal cortex reveal discrete steps during decision-making". *Science,* 351**,** 1406.

SHADLEN, M. N. & NEWSOME, W. T. 2001. Neural Basis of a Perceptual Decision in the Parietal Cortex (Area LIP) of the Rhesus Monkey. *J Neurophysiol,* 86**,** 1916-1936.

SONG, J. H. & MCPEEK, R. M. 2010. Roles of narrow- and broad-spiking dorsal premotor area neurons in reach target selection and movement production. *J Neurophysiol,* 103**,** 2124-38.

THURA, D., BEAUREGARD-RACINE, J., FRADET, C.-W. & CISEK, P. 2012. Decision making by urgency gating: theory and experimental support. *Journal of Neurophysiology,* 108**,** 2912.

THURA, D. & CISEK, P. 2014. Deliberation and commitment in the premotor and primary motor cortex during dynamic decision making. *Neuron,* 81**,** 1401-16.

THURA, D. & CISEK, P. 2016. Modulation of Premotor and Primary Motor Cortical Activity during Volitional Adjustments of Speed-Accuracy Trade-Offs. *J Neurosci,* 36**,** 938-56.

VAADIA, E., KURATA, K. & WISE, S. P. 1988. Neuronal activity preceding directional and nondirectional cues in the premotor cortex of rhesus monkeys. *Somatosens Mot Res,* 6**,** 207-30.

VICKERS, D. 1970. Evidence for an Accumulator Model of Psychophysical Discrimination. *Ergonomics,* 13**,** 37-58.

WANG, M., CHANDRASEKARAN, C., PEIXOTO, D., NEWSOME, W. T. & SHENOY, K. V. Dorsal premotor cortex activity reflects a candidate decision variable during the action selection epoch of an abstract perceptual decision-making task Society For Neuroscience, 2016 San Diego, CA.

1133 WANG, X.-J. 2002. Probabilistic Decision Making by Slow Reverberation in
1134   Cortical Circuits. *Neuron,* 36**,** 955-968.
1135 WISE, S. P. 1985. The primate premotor cortex: past, present, and preparatory.
1136   *Annu Rev Neurosci,* 8**,** 1-19.
1137 WISE, S. P., BOUSSAOUD, D., JOHNSON, P. B. & CAMINITI, R. 1997. PREMOTOR
1138   AND PARIETAL CORTEX: Corticocortical Connectivity and Combinatorial
1139   Computations1. *Annual Review of Neuroscience,* 20**,** 25-42.
1140 WONG, K.-F. & WANG, X.-J. 2006. A Recurrent Network Mechanism of Time
1141   Integration in Perceptual Decisions. *The Journal of Neuroscience,* 26**,** 1314.
1142
1143

Methods

1145

Subjects

1147

1148 Our experiments were performed on two adult male macaque monkeys (*Macaca*
1149 *mulatta*) trained to perform a direction discrimination task with reaching movements
1150 of the arm as operant responses. Neural activity was recorded from populations of
1151 neurons in dorsal premotor and primary motor cortex while monkeys performed the
1152 task. All training, surgery, and recording procedures conformed to the National
1153 Institutes of Health Guide for the Care and Use of Laboratory Animals and were
1154 approved by Stanford University Animal Care and Use Committee.

1155

Apparatus

1157

1158 Monkeys sat in a primate chair in front of a video touchscreen, with their head
1159 restrained using a surgical implant. The front plate of the chair could be opened,
1160 allowing the subjects to reach the touchscreen with the arm contralateral to the
1161 implanted hemisphere. The ipsilateral arm was gently restrained using a delrin tube
1162 and a cloth sling. Stimuli were shown on the video touchscreen (ELO Touchsystems
1163 1939L), which allowed us to track hand position at 75Hz and was positioned
1164 approximately 35 cm away from the monkeys' head. Eye position was continuously
1165 tracked with an optical eye tracker at 1kHz (EyeLink 1000, SR Research, Canada).

1166

Motion Discrimination Task

1168

1169 The task employed is a variation of the classical dots discrimination task, in which
1170 arm movement was the operant response (Fig. 1a). We used two variants of this task
1171 that differed based on the stimulus duration employed. The first version was a
1172 classical fixed duration task, in which every stimulus presentation lasted 1000 ms. We
1173 termed this version the fixed duration task. In contrast, we also employed a version in
1174 which the duration of the stimulus presentation varied from trial to trial. The stimulus
1175 duration ranged from 200-1000 (median 435 ms) and it was randomly chosen on each
1176 trial by sampling an exponential distribution. We termed this version, the variable
1177 duration task. For all variants, the trial starts with the onset of a fixation point (FP; 1.5
1178 degree diameter) on a video touchscreen (Fig. 1a). To initiate the task, the monkey
1179 was required to maintain both eye and hand fixation within +/- 3 degrees of the FP as
1180 long as it remained on the screen. Importantly, throughout the entire trial, the monkey
1181 was required to always maintain direct hand contact with the screen, otherwise the
1182 trial would be aborted.

1183
1184 After 300 ms of fixation, two targets (1.5 degree diameter) appeared on opposite sides
1185 of and at same distance from the FP. After a 500 ms delay the random dot stimulus
1186 was presented for either 1000 ms (fixed duration) or 200-1000 ms (variable duration),
1187 depending on the task variant, after which it was removed from the screen. On each
1188 trial a fraction of the dots moved coherently along the horizontal axis in the 0 and 180
1189 degree directions. The monkey was asked to report the net direction of motion by
1190 reaching to the target in the corresponding direction. The difficulty of the task was
1191 adjusted by changing the fraction of dots moving coherently in one direction (motion
1192 strength) (Britten et al., 1992). After the stimulus offset the monkey either entered a
1193 delay period during which it was required to withhold his response for 400-900 ms
1194 (for the fixed duration task) or was immediately presented the go cue (variable
1195 duration task). The go cue was then signaled by the offset of the FP at which point the
1196 monkey was free to gaze anywhere and report his decision by reaching to one of the
1197 two targets. Although gaze was monitored, reward acquisition depended solely on
1198 reaching to the correct target. Finally, for a response to be considered valid, the
1199 monkey was required to hold its hand position within +/- 4 degrees of the center of
1200 the target for 200 ms. The monkey was then rewarded with a drop of juice for correct
1201 choices and given a timeout (2-4 seconds) for incorrect ones. Zero coherence trials
1202 were rewarded randomly with a probability of 0.5 since there was no correct response
1203 on these trials.
1204
1205 **Random dots stimuli**
1206
1207 The stimuli used in our psychophysical experiment were random dot kinematograms
1208 (RDK) generated using MATLAB and Psychophysics Toolbox. Stimuli were
1209 presented on a 19-inch LCD touch monitor (Elo Touchsystems) with 75 Hz frame rate
1210 and 800 x 600 pixels resolution positioned 30 cm away from the monkey. The details
1211 for generating the random dots stimuli have been described previously (Kiani et al.,
1212 2008). We used the same algorithm and parameters except: (1) the stimulus duration
1213 was fixed at 1 s for the fixed duration task and variable from 0.2s -1s (exponentially
1214 distributed) in the variable duration task; (2) the diameter of the stimulus aperture was
1215 14 degrees, and (3) the speed of the coherent dots was 8 degrees / second. The dot
1216 density was 16.7 dots/deg^2/s, and the dot size 2 pixels. The center of the dots stimulus
1217 was situated 12 degrees above the center of the fixation point. To create the
1218 impression of motion, the dots in the RDK were split into 3 consecutive sets with the
1219 same number of elements (1 set displayed for each individual frame) and displaced 3
1220 frames (40 ms) later. The fraction of dots displaced coherently toward one of the two
1221 targets was determined by the coherence (motion strength), with the remaining dots
1222 being displaced randomly. For both monkeys, the motion strength could take one of 6
1223 possible values: 0%, 3.2%, 6.4%, 12.8%, 25.6% and 51.2%. The direction and
1224 coherence of the motion were randomly assigned on each trial by sampling from a
1225 uniform distribution with replacement. For zero-coherence stimuli all dots were
1226 displaced randomly but, due to the stochasticity of that process, one obtains non-zero
1227 net motion toward the targets over a small number of frames.
1228
1229 **Behavioral Training**
1230
1231 Training two monkeys to perform all versions of the dots discrimination task with
1232 excellent behavior required a thorough operant conditioning protocol. The protocol

25

had to be adapted to the individual monkeys since they had very different training histories: monkey H was a naive monkey whereas monkey F had been trained on a saccade version of the motion discrimination fixed duration task. Monkey H started by being rewarded just for touching the touchscreen and then gradually progressed to an instructed reach task and from there to a delayed reach task. Once he was proficient in using the touchscreen, the dots stimulus was introduced, cueing the correct target to reach to at the end of the trial. Only easy coherences were used at first, with lower and lower coherences being introduced gradually until the final set was used. The final component of training was eye fixation. Eye fixation was trained by introducing blocks of trials for which the front plate of the primate chair was closed, cueing the monkey to perform the task with eye movements. The fixation window size was gradually decreased, and then eye fixation was also required during the reach blocks. By aborting trials if eye or hand fixation was broken the subject learned that both were required to perform the final task. Monkey F on the other hand was already proficient at discriminating motion so the main focus of training was achieving proficient use of the touchscreen with his hand. The same initial sequence of steps was used to train monkey F to perform delayed reaches. From that point on, the training was focused on combining knowledge about the dots task with the reaching response. Coherences were also introduced sequentially from highest to lowest but at much faster pace compared to monkey H. Recording sessions started when good psychophysical performance was achieved.

Behavioral Analysis

Psychophysical performance was assessed in two ways: by describing the percentage of correct choices as a function of (unsigned) stimulus coherence and by describing the percentage of right choices as a function of signed stimulus coherence.

The percentage of correct choices as a function of motion strength (stimulus coherence) was fit by a cumulative Weibull distribution function (equation 1):

$$P_{correct}\ (c) =\ 1 - 0.5 \times e^{(-\frac{c}{\alpha})^{\beta}}$$

where $P_{correct}$ is probability correct, c is motion strength, α is the psychophysical threshold (the value of c that corresponds to ~82% correct responses), and β is a parameter that controls the shape of the function, especially its steepness.

The percentage of rightward choices, P_{right}, as a function of motion strength and direction was fit by a logistic regression (equation 2):

$$P_{right}\ (c) =\ \frac{1}{1 +\ e^{-\beta_1 \times (\beta_0 + c)}}$$

where c is signed motion strength, β_1 is the slope parameter and, $-\beta_0$ is the motion strength corresponding to the indifference point. This value was used to assess the monkey's behavioral bias on each session.

To analyze performance as a function of stimulus duration (Fig. 1d) trials in the variable duration task were ranked by stimulus duration, binned and fitted with

26

1280 Weibull curves. In the y-axis we plot the α (threshold) parameter ($\log_2$ scale) obtained
1281 from the fits for each set of trials, and in the x-axes the median duration of the
1282 stimulus for each bin ($\log_2$ scale).
1283
1284 For a perfect integrator threshold should decrease linearly with stimulus duration (in
1285 $\log_2$ vs $\log_2$ plot) with a slope of -0.5 (Kiani et al., 2008). To assess at what point the
1286 observed decrease in threshold deviated from that expected for the perfect integrator
1287 we performed bi-linear fits to the data. We forced the first slope to be -0.5 and let the
1288 intercept, the second slope and the time of slope change as free parameters. The time
1289 of slope change obtained from the fits indicates the point at which behavioral
1290 improvement deviates significantly from the perfect integrator prediction. For the
1291 regression analyses we used independent bins of 500 trials. For Figure 1d we show
1292 bins of 500 trials that are incremented by 250 trials to interpolate the data and guide
1293 the eye.
1294
1295 In addition to psychophysical performance two behavioral metrics related to the arm
1296 reach itself were also quantified: reaction time (RT) and hand velocity. To obtain
1297 precise measurements of reaction times and maximum hand velocity we used the raw
1298 hand position data on each trial. We started by up-sampling the raw data by a factor of
1299 13 to obtain artificial 1 ms resolution (since it had been acquired at 75Hz). Then we
1300 smoothed the up-sampled data by performing local linear regression to obtain smooth
1301 hand traces for each trial. The instantaneous velocity was calculated as the norm of
1302 the sum of vertical and horizontal speed components (the instantaneous derivative of
1303 the position). The peak hand velocity was calculated for each trial and reaction time
1304 was determined as the interval between the presentation of the go signal and the time
1305 point at which 20% of the peak velocity was reached.
1306
1307 **Electrophysiological recordings**
1308
1309 Two multielectrode arrays (Blackrock Microsystems, Utah) with 96 electrodes each
1310 (1mm long platinum-iridium electrodes, 0.4 mm spacing, impedance 400 kOhm) were
1311 implanted in primary motor and dorsal premotor cortex of each monkey (Figure 1e).
1312 The arrays were placed anterior to the central sulcus, posterior to the arcuate sulcus
1313 and lateral but near the superior pre-central dimple (Churchland et al., 2010). Prior to
1314 the array implantation, single electrode recordings were performed (FHC, Maine) by
1315 lowering dura-piercing electrodes (tungsten, average impedance 6 MOhm) through
1316 burr holes, to determine the best location for the arrays. M-L position was determined
1317 by performing muscle palpation during recordings and searching for a strong upper
1318 arm representation; A-P position was determined by strong perimotor/delay activity in
1319 a delayed reach task for M1/PMd, respectively. The coordinates for the best sites were
1320 calculated with respect to the center of the chamber and verified during surgery using
1321 stereotaxic measurements. These coordinates were used to determine the final
1322 location of the arrays, subject to anatomical constraints (curvature of the cortex, blood
1323 vessels etc). Continuous neural data were acquired and saved to disk from each
1324 channel (sampling rate 30 kHz) and thresholded at -4.5 RMS. Waveforms
1325 corresponding to threshold crossings were sorted offline (Plexon Inc., Dallas) using
1326 both semi-automatic clustering methods and manual sorting. For all analyses
1327 presented in this study we did not differentiate between single-units and multi-units.
1328 Our goal was to maximize population predictive power and spatial coverage of the
1329 cortex and not just to select the very best isolated single-units. Only units with an

1330 average firing rate of 2 spikes/s or more during dots presentation were analysed in this
1331 study. The number of units meeting this criterion in each experimental session
1332 typically ranged from 100-180 per array.
1333
1334 **Datasets**
1335
1336 For each task version and monkey we analyzed all datasets from each brain area that
1337 met two behavioral inclusion criteria: 1) over 750 trials and 2) a behavioral bias ($|\beta 0|$)
1338 under 5%, as determined by a logistic regression fit. These criteria were imposed to
1339 guarantee that we have a sizeable number of trials per condition (6 coherence x 2
1340 directions = 12 conditions) and that the behavior of the monkey is minimally biased,
1341 such that both neural and behavioral results are more easily interpretable. These
1342 criteria resulted in a selection of 9 (12) sessions of the fixed duration task and 6 (5)
1343 sessions of the variable duration task with no delay for monkey H (F), respectively.
1344 Data from both areas were collected simultaneously and the same recording sessions
1345 were used.
1346
1347 **Peri-stimulus time histograms (PSTHs)**
1348
1349 PSTHs were generated by aligning spike trains of each trial to relevant task events:
1350 target onset, stimulus onset, go cue, and movement initiation. These spike trains were
1351 then convolved with a Gaussian kernel with a 50 msec acausal and a 50 ms causal
1352 component. The standard deviation of the Gaussian used was 30 msec. The resulting
1353 spike density functions were then sorted by experimental condition. Once the trials
1354 were selected for the specified condition, their spike density functions were averaged.
1355
1356 **Logistic Regression**
1357
1358 For each session, the responses of all neurons in 90% of the trials were fit with a
1359 logistic model that attempted to separate rightward (T1) and leftward (T2) upcoming
1360 choices. The logistic model was fit in 50 ms windows, advanced in 20 ms steps over
1361 the entire trial duration (equation 3).
1362

$$P(T_1|\vec{r}) = \frac{1}{1 + e^{-(\beta_0 (t) + \sum_{i=1}^{n} \beta_i(t) \times r_i(t))}}$$

1363
1364 Where $P(T_1|\vec{r})$ is the probability of observing a particular behavioral choice (T_1 or
1365 rightward choice in this case) given the population response $\vec{r}$; $r_i(t)$ are the z-scored
1366 summed spike counts for each neuron and time window, β_0 is an intercept term and
1367 $\beta_i(t)$ are the classifier weights (one for each neuron and time window).
1368
1369 The remaining 10% of the trials were tested using the previously trained model and its
1370 accuracy was recorded. The same process was followed 10 times for each window
1371 (10-fold cross-validation) and the percentage of correctly predicted choices recorded.
1372 This process was repeated for consecutive windows displaced by 20 ms and yielding a
1373 prediction accuracy trace for each session and brain area. Both correct and error trials
1374 were included in this analysis to assure there would not be an imbalance between high
1375 coherence trials (more likely to be correct trials) and low coherence trials, which
1376 would bias the classifier to perform better on high coherence trials.
1377

An L1- regularization technique (LASSO) was used to constrain the norm of the beta coefficients fitted by the model to prevent over-fitting (Kiani et al., 2014b). The lambda parameter that determines the strength of the penalty for the L1 norm was calculated for the 50 ms window preceding the go-cue by sweeping through 25 potential values and selecting the value with lower deviance by running 10-fold cross validation. This lambda value was then used for the model for all time points.

The exact same procedure was also followed using 150 ms windows (instead of 50 ms) to test whether choice prediction accuracy could still further improve, when applying an identical logistic regression method to the same datasets.

Finally, a slightly different procedure was used when training a single classifier over an entire epoch. The four epochs used for training the four corresponding classifiers were:

 • Targets epoch: [-150, 350] ms aligned to targets onset;

 • Dots epoch: [150, dots offset] ms aligned to dots onset. Dots offset was 1000 ms for fixed duration task and between 200-1000 ms for the variable duration task;

 • Delay/Pre-Go epoch: [-600, 0] ms aligned to go cue;

 • Peri-movement epoch: [-200, 600] ms aligned to reach;

All valid 50 ms samples of neural data during the selected period (above) for each epoch were used as a sample to train the corresponding classifier. The classifier was trained on 90% of the trials and tested on 10% of the trials using 10-fold cross-validation. As before, LASSO regularization was used to prevent over-fitting. The regularization parameter lambda was calculated individually for each epoch through cross-validation and chosen as the value with minimum expected deviance. Accuracy was calculated as fraction of test trials correctly predicted at every 50 ms long window (stepped in 20 ms increments).

Coherence effects on prediction accuracy

For each dataset, coherence effects were assessed by measuring the difference in prediction accuracy between consecutive coherence levels: (51.2%-25.6%), (25.6%-12.8%), (12.8%-6.4%), (6.4%-3.2%), (3.2%-0%). Five 200 ms long periods during the dots presentation were considered. For each period, the five differences in prediction accuracy were averaged across time. Results for each period, brain area and task were combined across datasets. The Wilcoxon signed rank test ($p<0.005$) was used to assess if coherence accuracy differences were considered significantly larger than 0. The same criterion was used to assess significance of differences in coherence effects magnitude between brain areas within the same time period.

Latency analysis

We determined the latency for choice predictive signals during the dots period as the first of three consecutive (and non-overlapping) 50 ms time steps for which the prediction accuracy is significantly larger than chance (0.5) according to a Wilcoxon signed rank test, $p<0.001$.

29

Decision Variable

When performing logistic regression on the population activity, the set of weights associated with each neuron form the hyperplane that best separates leftward and rightward choices for the corresponding time window (50 ms width at a time). For each trial and time point, the distance of the population state to this hyperplane is given by the model choice log odds, i.e. it corresponds to the model's certainty about the upcoming choice of the monkey—the further from the hyperplane, and thus the larger the distance, the higher the confidence of the model on its estimate of the eventual choice of the animal (equation 4):

$$DV = \log \frac{P(T_1|\vec{r})}{P(T_2|\vec{r})} = \beta_0(t) + \sum_{i=1}^{n} \beta_i(t) \times r_i(t)$$

Where $r_i(t)$ are the z-scored summed spike counts for neuron i and time window t, $\beta_0(t)$ is an intercept term and $\beta_i(t)$ are the classifier weights (one for each neuron and time window). We use this distance as a proxy for an internal decision variable (DV) and study its dynamics as a function of stimulus difficulty and trial epoch. Using longer time windows of neural activity as predictors of choice increased the accuracy even further (Supp. Fig. 5a) at the expense of time resolution.

Slope Analysis

To analyze the dependency of our putative decision variable on the stimulus strength we fit the single trial DV traces with a tri-linear curve. Data in the interval [0-500] ms aligned to dots onset was used to fit the curves. For the variable duration task no data after the go-cue was presented was used in this fit. We fix the first slope at zero since the stimulus does not influence the neural representation of choice within the first ~100-150 ms following stimulus onset. The intercept, the 2nd and 3rd slopes, as well as the transition times are all free parameters. All free parameters were fit to minimize squared error. We used the value of the 2nd slope to quantify the DV initial rate of rise due to motion information. Since the subsequent analyses focused on this parameter, variable duration trials with stimulus duration in the [200,500] ms range were also used.

The curves were fitted independently for each trial and the fitting procedure was blind to stimulus coherence or task variant. Only correct trials were used in this analysis. Within each task we then tested if the slopes resulting from the fitting procedure had a statistically significant dependence on coherence. We did this in two ways: 1) by regressing slopes as a function of stimulus coherence and 2) by regressing slopes as a function of log2(stimulus coherence). The results were similar in both cases.

Finally we tested the effect of coherence, task variant, and their interaction on slopes across tasks for each brain area and target direction by fitting the following model:

$$DV_{slope} = \beta_0 + \beta_1 \times C + \beta_2 \times I + \beta_3 \times C \times I$$

Where DV_{slope} is the 2nd slope, C is the magnitude of the stimulus coherence, normalized to 1 and I is the task identity (0 for fixed duration, 1 for variable duration).

1472

1473 The resulting β_0 is the intercept term, β_1 quantifies the effect of coherence on slopes
1474 (across tasks), β_2 quantifies the shift in slope magnitude between tasks (across
1475 coherences) and β_3 captures the coherence dependency of the offset of the slopes
1476 between tasks. A significant and positive/negative β_1 value would indicate slopes
1477 increase/decrease as a function of coherence, a significant and positive β_2 value
1478 would imply slopes are higher for the variable duration task compared to the fixed
1479 duration task (across coherences), and a significant and positive β_3 value would imply
1480 the offset between variable duration and fixed duration slopes is coherence dependent.

1481

1482 All slope analyses were done on correct trials only to assure coherence effects were
1483 not a result of including higher number of incorrect trials for low coherences.

1484

1485 **Behavioral metrics prediction**

1486

1487 We attempted to predict/explain four behavioral metrics based on neural activity
1488 throughout the trial: hand reaction time, eye reaction time, hand peak velocity and eye
1489 peak velocity.
1490 To predict hand or eye Reaction Time (RT) based on neural activity we performed
1491 Ridge regression on the z-scored firing rates of all units within a 150 ms window
1492 according to:

1493

$$RT_i = \beta_0(t) + \sum_{i=1}^{n} \beta_i(t) \times r_i(t)$$

1494
1495
1496 Where RT_i is the behavioral reaction time on a given trial, n is the number of units,
1497 $r_i(t)$ is response of unit i at time t and the β coefficients are the fit model parameters.
1498 For each window, a different model was trained for each reach direction (left and
1499 right) on 90% of the correct trials that lead to the corresponding choice. Then the RTs
1500 on the remaining 10% of the trials were estimated using the trained model and the
1501 units firing rates. We performed this same process 10 times for each window (10-fold
1502 cross validation) and obtained a set of estimated Reaction Times. We then performed
1503 a linear regression between the estimated and the observed reaction times for all trials
1504 and recorded the R-squared value. Finally, we slid the window by 20 ms and repeated
1505 the process until all relevant epochs of the trial were tested. The adequate Ridge
1506 parameter was estimated independently for each dataset and reach direction for the
1507 window comprising [200, 350ms] after the Go cue, where the RT signal tended to be
1508 strongest. The estimation was performed using 10-fold cross validation over 20
1509 potential values. The value corresponding to the smallest testing error was chosen and
1510 used to regularize the linear model in every window. The exact same procedure was
1511 followed when attempting to predict hand and eye peak velocity. Trials with hand RT
1512 lower than 150 ms or higher than 800 ms were excluded from this analysis.

1513

1514 **Integration models**

1515

1516 We investigated which variations of the integration-to-bound models could potentially
1517 explain changes in the dynamics of single trial DVs in the fixed and variable duration
1518 tasks. To contrast quantitative predictions of these models, we implemented a basic
1519 integration model and its three key variants for acceleration of choice representation

1520 by changing input gain, urgency, and recruitment of choice-representing units. The
1521 basic model assumes that two large neural populations integrate sensory evidence in
1522 favor of the two competing choices. Each integrator receives two types of inputs. The
1523 first is the momentary evidence about motion:

$$e(t) = s(t) \times g(t)$$

1524 where $s(t)$ is a random draw from a Gaussian distribution and $g(t)$ is a gain term that
1525 scales the input of the integrator. The mean of the Gaussian distribution of $s(t)$ is
1526 $k \times C$ for one integrator and $-k \times C$ for the second integrator, where C is the signed
1527 motion coherence in a trial, and k is the sensitivity coefficient for motion on the
1528 display monitor. The linear dependence of the mean of momentary evidence on
1529 motion strength is compatible with neural responses in motion selective areas MT and
1530 MST (Britten et al., 1996, Celebrini and Newsome, 1994). The standard deviation of
1531 the Gaussian distribution is 1. The second input to the integrators is an urgency signal
1532 that drives both integrators toward their bounds. The accumulated evidence is:

$$v(t) = \int \big(e(t) + u(t)\big)\, dt$$

1533 Each integrator has a lower reflective bound B_l and an upper absorbing bound B_u
1534 (Kiani et al., 2014a). The integration continues until one of the integrators reaches the
1535 upper bound. At that time, a choice is made and the two integrators maintain their
1536 states until the end of the motion presentation period. The model shows a monotonic
1537 improvement of choice accuracy with motion strength, consistent with the monkey's
1538 behavior.
1539
1540 To mimic our recordings, we simulated 100 spiking units from each of the two
1541 integrator populations. The spikes were generated based on an inhomogeneous
1542 Poisson process. The instantaneous firing rate of each unit at each moment in a trial
1543 was a weighted average of the accumulated evidence and a choice-representing
1544 signal:

$$r_i(t) = \alpha_i v(t) + \gamma_i \Im(t)$$

1545 where $r_i(t)$ is the firing rate of unit i at time t. α_i and γ_i are weights between 0 and 1
1546 and determine the tuning of the neuron for representing integrated evidence and
1547 choice. The choice representing signal, $\Im(t)$, is assumed to be a monotonic function
1548 created by a non-linear transformation of $v(t)$. We chose an accelerating function
1549 based on distance of accumulated evidence from the decision bound (B_u)

$$\Im(t) = \begin{cases} \rho_{max}\Phi(v(t), B_u, \sigma) & for\ v(t) < B_u \\ \rho_{max} & for\ v(t) \geq B_u \end{cases}$$

1550 where $\Phi(.)$ is a cumulative Gaussian function, ρ_{max} sets the maximum of $\Im(t)$, and
1551 σ determines the rate of acceleration. Introducing more realism by allowing response
1552 correlations, similar to those observed in electrophysiological recordings, or testing
1553 other monotonic functions did not significantly change our conclusions about the
1554 models.
1555
1556 We simulated 3000 trials for each motion direction and coherence, saved the spike
1557 times of the units, and used a logistic regression to calculate the single trial DVs, just
1558 as we did for the PMd and M1 neural responses. For the base model and its gain and
1559 urgency variants, γ_i were set to 0, making the units represent only the accumulation of
1560 evidence. For the progressive recruitment model, γ_i could take any value between 0
1561 and 1, making the neurons represent a mixture of accumulated evidence and
1562 categorical choice signal. α_i and γ_i where chosen independently. For the simulations
1563 presented in this paper, the parameters of the base model were $k = 0.3$, $g(t) = 1$,

1564 $u(t) = 0$, $B_l = -5$ and $B_u = 20$. The same parameters were used for the progressive
1565   recruitment model, while ρ_{max} was set to 40. For the model with high input gain,
1566 $g(t)$ linearly increased from 1 to 3 over 1000ms. For the model with low gain, $g(t)$
1567   grew from 1 to 1.25. For both models $u(t)$ was 0. For the models with low and high
1568   urgency, $u(t)$ was 0.005 ms^{-1} and 0.025 ms^{-1}, respectively, and $g(t) = 1$. Our
1569   conclusions are not critically dependent on these specific numbers and hold for a wide
1570   range of model parameters, as long as the upper absorbing bound is low enough to
1571   curtail the integration process, compatible with the monkeys' behavior (Fig. 1).
1572   Simulations of the integration process and spiking of the model units were done with
1573   1ms time steps.
1574
1575   **Stability of the population choice vector**
1576
1577   For each dataset, we divided the trials in two disjoint sets. Within each set of trials,
1578   we then modeled the (z-scored) firing rate of each unit at each point as a linear
1579   combination of task related predictors (equation 9):
1580

$$r_i(t) = \beta_0 + \beta_{coh} \times coh_i + \beta_{choice} \times choice_i + \beta_{difficulty} \times difficulty_i$$

1581
1582   Where β_0 is the intercept term, coh_i is the signed stimulus coherence on trial i. (1 for
1583   51.2% rightward motion and -1 for 51.2% leftward motion), $choice_i$ is the behavioral
1584   choice on trial i (1 right choice and -1 for left choice) and $difficulty_i$ is the absolute
1585   stimulus coherence on trial i (1 for 51.2% trials and 0 for 0% trials)
1586
1587   At every 10 ms interval, we obtained a β_{choice} coefficient for each unit. We
1588   concatenated these values for all units into a vector $\vec{\beta}_{choice}$ and normalized it. We
1589   repeated this same procedure across all time points and obtained a matrix $B_{1,choice}$.
1590   We then followed the exact same steps for the second set of trials and obtained a
1591   second matrix $B_{2,choice}$. Next, we projected $B_{1,choice}$ onto $B_{2,choice}$ to obtain a cross-
1592   validated measure of vector alignment (dot product) matrix. Because $B_{1,choice}$ and
1593 $B_{2,choice}$ were calculated using disjoint sets of trials the diagonal values are
1594   meaningful and not set to 1 by convention (Fig. 6, Supp. Figs 16 and 17). To further
1595   average out spurious vector alignment when the choice signal is small, for each
1596   dataset we performed the dot product matrix calculation 20 times always starting from
1597   different sets of trials. We then averaged the dot product matrices across iterations
1598   and finally across datasets within each condition (brain area, task - Fig. 6a-d, Supp.
1599   Figs 16 and 17). For the comparison across tasks we used data from 3 sessions in
1600   monkey F for which we collected data on the fixed duration task and the variable
1601   duration task back to back (Fig. 6e-f). In total, these sessions comprised 1425 trials in
1602   the fixed duration task and 2466 trials in the variable duration task. For these sessions,
1603   neural activity was hand sorted and only channels with waveform shapes deemed
1604   stable and easily identifiable in both blocks of trials were included in the analyses.
1605   The sorting procedure was done prior and without knowledge of the results of the
1606   choice stability analyses. The median average of channels excluded this analysis was
1607   only 8 out of up to 96 channels.
1608
1609   The analysis of the stability of the population choice vector could have been
1610   implemented using the discriminant hyperplanes obtained from the logistic regression
1611   analysis. However, we instead performed the linear regression described above for

1612 two reasons. First, the beta values for the discriminant hyperplane are obtained using
1613 aggressive L1 regularization, which pushes the lowest weights to zero to improve
1614 prediction accuracy and avoid overfitting. The logistic classifier could underestimate
1615 the contribution of neurons with small but significant choice representation especially
1616 late in the trial when strong choice selectivity arises in the population. This scenario
1617 would lead to "artificially" lower dot product of the choice axes across time. Instead
1618 we used three regressors in our linear model for choice, signed motion strength and
1619 absolute motion coherence. The choice regressor will capture the choice
1620 representation while the signed motion regressor will capture motion related signals
1621 that are not fully explained by choice. Finally, we included a stimulus difficulty
1622 regressor that captures non-directional motion coherence signals whose presence has
1623 been reported in some LIP cells (Meister et al., 2013).
1624
1625 **Choice predictive units**
1626
1627 We applied the same linear model described above (equation 9) to model the (z-
1628 scored) firing rate of each unit at each time point and across all trials. For each time
1629 point we extracted a β_{choice} and an associated p-value. We considered a unit to be
1630 significantly modulated by choice if β_{choice} was significantly different from zero at
1631 five consecutive 10ms time points (p<0.05, Holm-Bonferroni corrected across all time
1632 points). The first of those data points was considered to be the onset of significant
1633 modulation for choice for that particular unit. We extended this analysis across all
1634 units within a dataset and calculated for each time point the cumulative fraction of
1635 units with significant choice modulation. The results were then averaged across
1636 datasets within the same condition (brain area, task).
1637
1638 To quantify how reliably each neuron predicted choice over time, we calculated the
1639 auROC (Shadlen and Newsome, 2001) metric for every 50 ms of the periods
1640 analyzed. According to our convention, right preferring neurons had 1 > auROC > 0.5
1641 and left preferring neurons 0 < auROC < 0.5 (Supp. Fig.24). To collapse across both
1642 choice directions, we calculated | auROC -0.5| (Fig. 7c-f). The units analyzed were
1643 collected in a session with both a fixed and variable duration block (monkey F) from
1644 channels whose waveforms were deemed stable (see above). For this representative
1645 session (Fig. 7c-f) only data from one channel in PMd and eight channels in M1 (out
1646 of up to 96) were excluded.
1647
1648 **Unit dropping**
1649
1650 For the unit dropping analysis we fit a logistic model (equation 3) to data obtained in
1651 the last 50 ms of dots presentation using 10-fold cross validation, just as before. The
1652 lambda regularization parameter however, was in this case fit to the same 50 ms
1653 epoch we would test (again using 25 potential values and 10-fold cross validation).
1654 The set of beta coefficients of the model corresponding to the lowest deviance lambda
1655 parameter was then chosen and ranked by magnitude. We removed from the data the
1656 unit with highest beta coefficient and re-trained and re-tested the model using 10-fold
1657 cross-validation and recorded the accuracy. This process was repeated 70 times until
1658 the 70 units with highest beta coefficients (ranked using the full model) were all
1659 dropped in descending order.
1660
1661
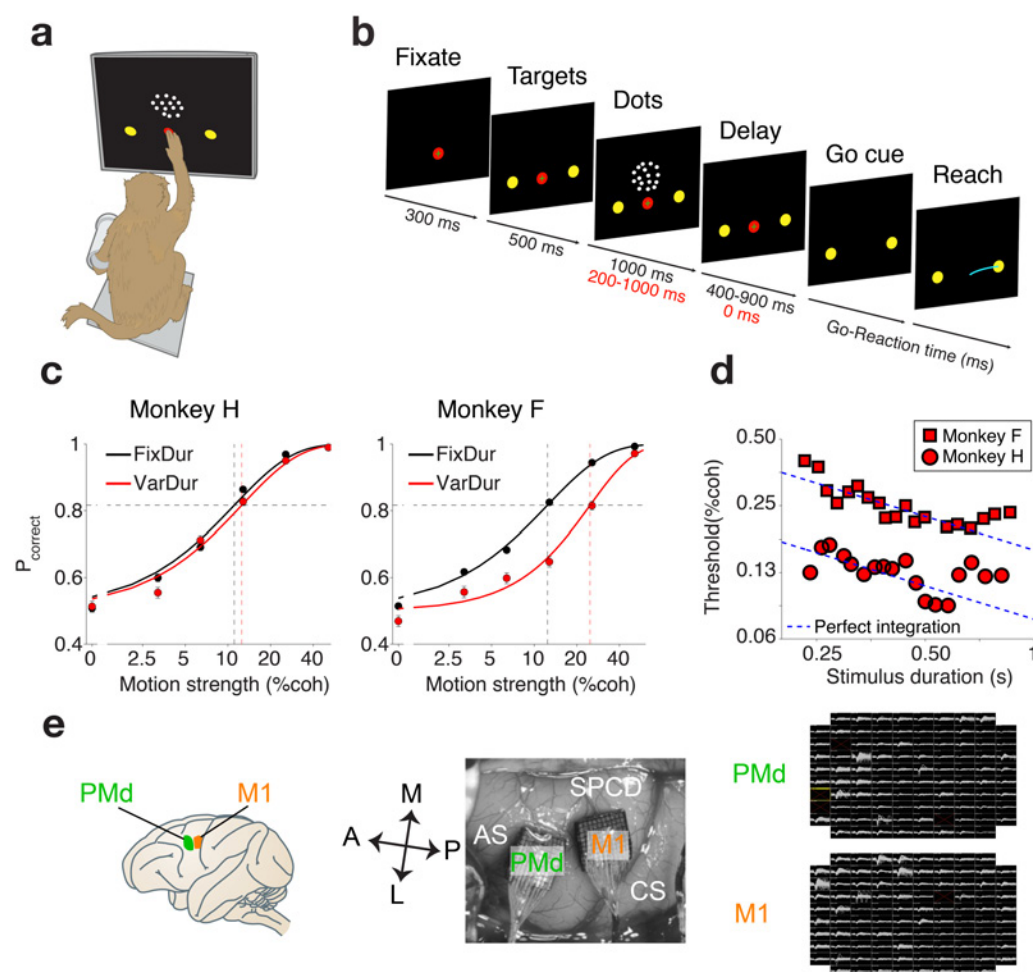
Figures

Figure 1 - Motion discrimination task, psychophysical performance and recording locations and techniques.

a) Behavioral setup - The monkey performed the motion discrimination task on a touchscreen using one arm, while the other arm remained gently restrained. Eye position was continuously tracked using an infrared mirror placed in front of the monkey's eyes.

b) Direction discrimination task structure - Trials start with the onset of a fixation point on the touchscreen. Once both eye and hand fixation are acquired two targets appear on the screen. The motion stimulus was shown after a short delay (500 ms) and lasted 1000 ms (200-1000 ms) for the fixed (variable) duration version. The dots offset was followed by a 400-900 ms delay in the fixed duration version whereas no delay was present for variable duration version. At the end of the delay, the offset of the fixation point cued the monkey to report his decision by making a hand reach movement to the appropriate target.

c) Psychophysical performance in the motion discrimination task. Percentage correct is plotted as a function of motion coherence for the fixed duration version (black) and the variable duration task (red) for monkey H (left panel) and monkey F

35

1685 (right panel). Observed data points (+/- SEM) are represented by the red and black
1686 markers. The data for each task was independently fit with Weibull curves (red and
1687 black curves). 17167/ 17440 trials for the fixed duration task and 4923/5381, trials for
1688 the variable duration task for monkey H/F, respectively.
1689 **d) Psychophysical thresholds in the variable duration motion discrimination**
1690 **task.** Psychophysical threshold is plotted as a function of stimulus duration for
1691 monkey H (circles) and monkey F (squares). Dashed blue lines show predicted perfect
1692 accumulation for each subject. The observed performance deviates from perfect
1693 accumulation for stimuli longer then 533/682 ms for monkey H/F respectively.
1694 **e) Location of the two multielectrode arrays.** Two 96 channel Utah arrays were
1695 implanted in primary motor and dorsal premotor cortex as judged by anatomical
1696 references (left and middle panels). Example waveforms collected from PMd and M1
1697 for the same experimental session (monkey H, right panel). White squares denote
1698 ground pins in the four corners of the arrays.
1699
1700

1701
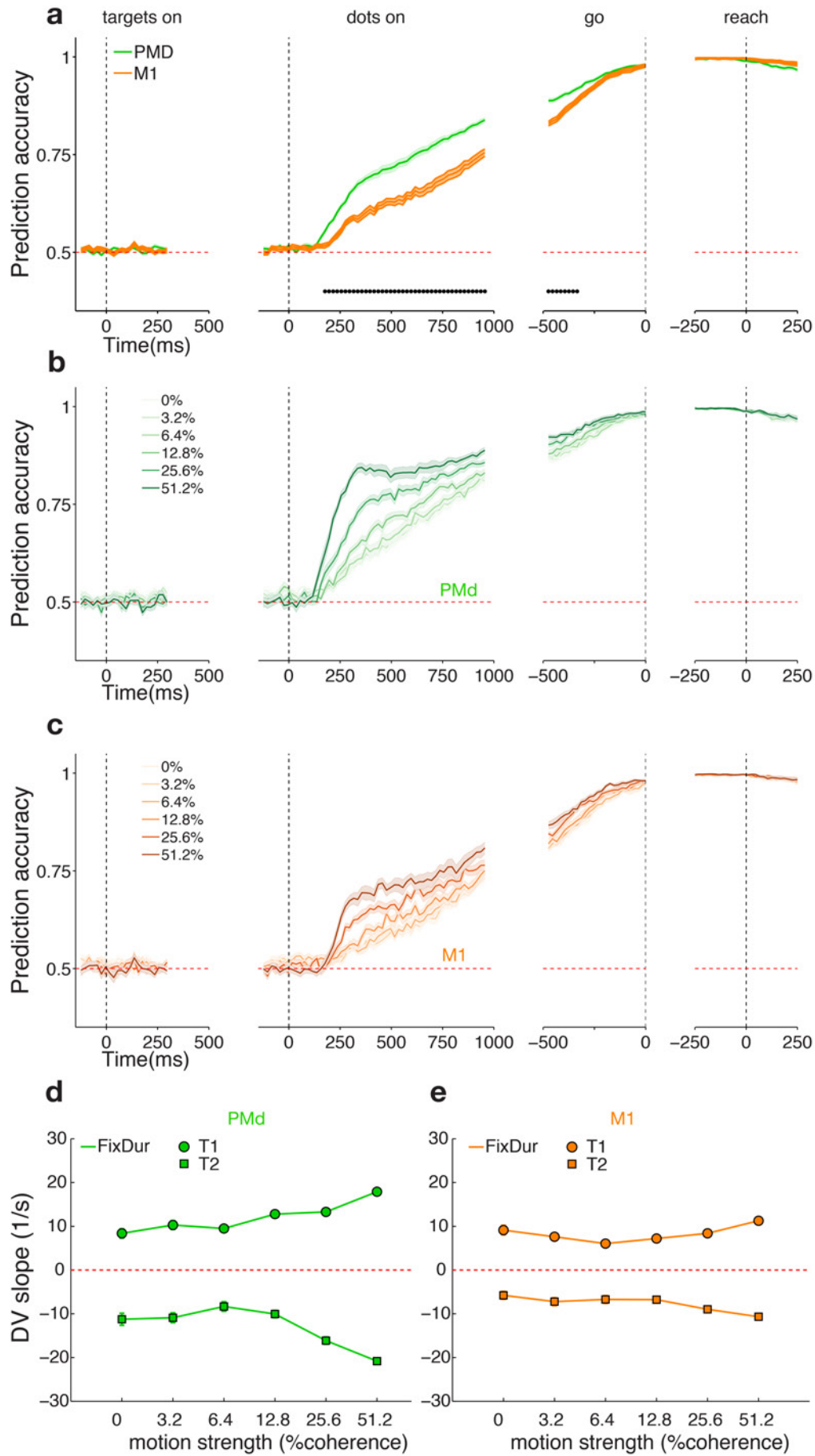
1702 **Figure 2 - Neural population choice prediction accuracy on single trials in the**
1703 **fixed duration task (pooled results across 2 monkeys).**
1704
1705 **a) PMd is more choice predictive than M1 during the stimulus presentation but**
1706 **not later in the trial.** Average prediction accuracy (see Methods) over time +- SEM
1707 for both monkeys. PMd (M1) data are plotted in green (orange). Black dots denote
1708 time bins for which the prediction accuracy was significantly different between the
1709 two areas (Wilcoxon signed rank test, p<0.05 Holm-Bonferroni correction for
1710 multiple comparisons).
1711 **b) Choice prediction accuracy in PMd rises faster for easier trials during**
1712 **stimulus presentation.** Average choice prediction accuracy as function of stimulus
1713 difficulty. Easy stimuli are represented in darker tones while harder stimuli are plotted
1714 in lighter tones, and shading corresponds to +- SEM. Same data as **a)** (green trace),
1715 except prediction accuracy is calculated individually for each stimulus difficulty.
1716 **c) Choice prediction accuracy in M1 rises faster for easier trials during stimulus**
1717 **presentation.** Same data as **a)** (orange trace), except prediction accuracy is calculated
1718 individually for each stimulus difficulty. Figure conventions as in **b).**
1719 **d) Single-trial decision variable slopes in PMd co-vary with stimulus coherence.**
1720 Average of single trial DV slopes are plotted as a function of stimulus coherence and
1721 choice. Positive values (circles) correspond to T1 (right) choices and negative values
1722 (squares) to T2 (left) choices (correct trials only). Error bars indicate +/- SEM across
1723 trials.
1724 **e) Single-trial decision variable slopes in M1 co-vary with stimulus coherence.**
1725 Same as **d)** for M1.
1726
1727
1728
1729
1730
1731
1732
1733
1734
1735
1736
1737
1738
1739
1740
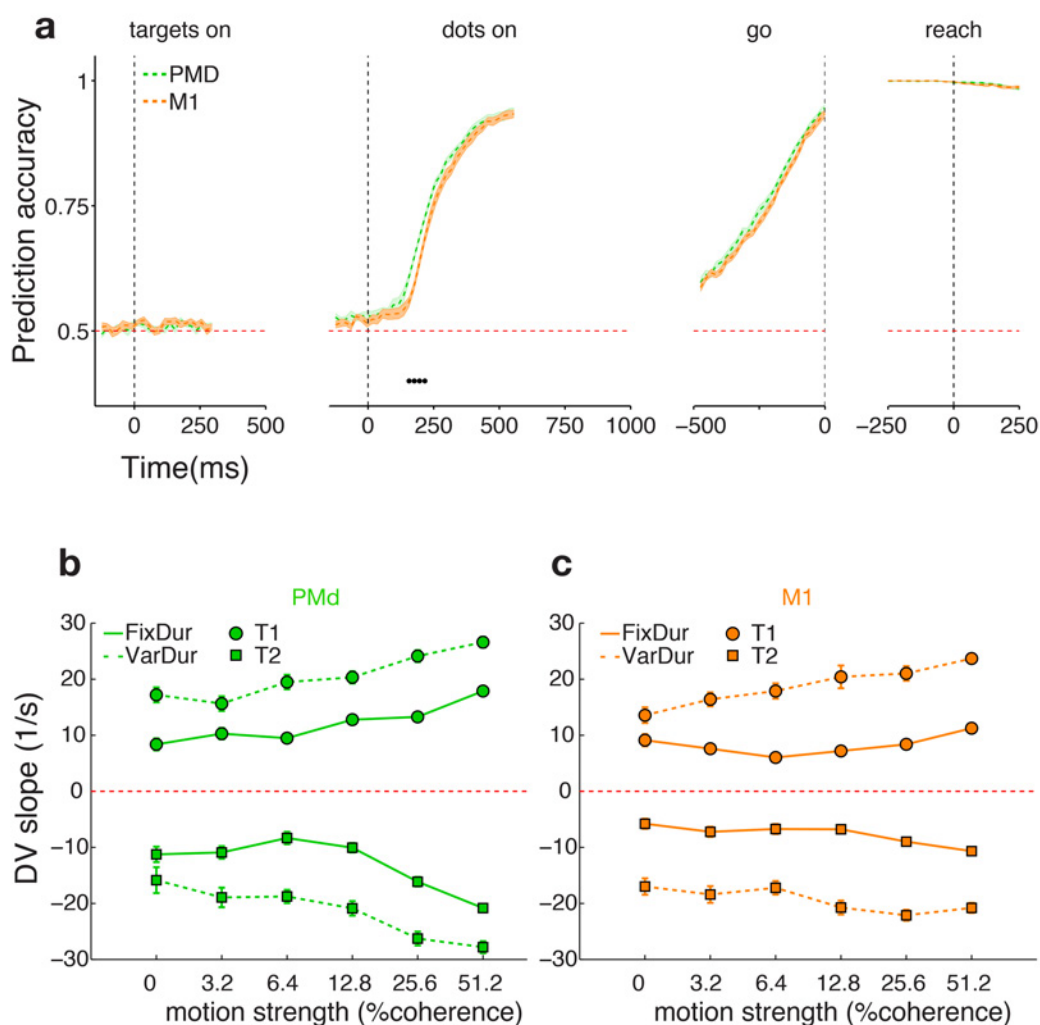
Figure 3 - Effects of stimulus duration uncertainty on choice prediction accuracy and model decision variable (pooled results across 2 monkeys).

a) Average prediction accuracy for variable stimulus duration sessions increases during the stimulus presentation. Equivalent to Figure 2a, but for variable stimulus duration sessions (same figure conventions). In the "dots on" panel, data were only included prior to the offset of the stimulus, ensuring that peri-movement activity did not affect the firing rates in this epoch. Because the visual stimulus varied in duration, fewer trials contribute to the trace as time progresses. In contrast to Figure 2a, prediction accuracy rises much faster and reaches higher values when the stimulus duration is uncertain. Differences between PMd and M1 dynamics are highly reduced under conditions of uncertainty.
b) Single-trial DV slopes for PMd increase for the variable duration task while maintaining co-variation with stimulus coherence. Data points show average single-trial DV slopes as a function of stimulus coherence and choice for variable stimulus duration (dashed lines) and fixed stimulus duration (solid lines, same data as Figure 2d) sessions. Error bars indicate +/- SEM across trials.
c) Single-trial DV slopes for M1 increase for the variable duration task while maintaining co-variation with stimulus coherence. Same as **b)** for M1. Figure

39

1763   conventions as in **b).**
1764
1765
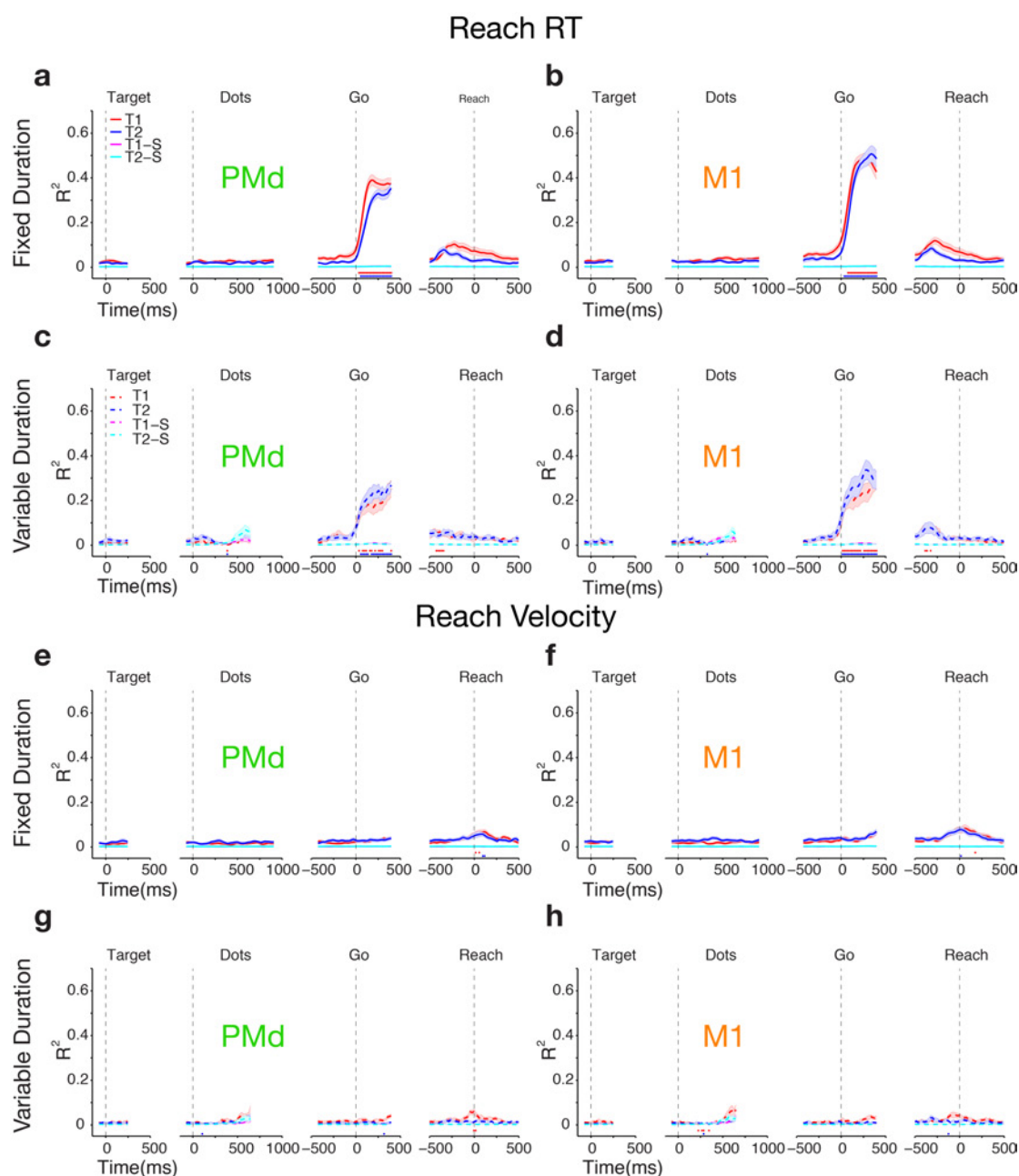
1766
1767
1768   **Figure 4 - Neural activity in PMd and M1 only becomes predictive of RT and**
1769   **hand velocity around the go-cue in both tasks (pooled results across 2 monkeys).**
1770
1771   **a) Fraction of variance explained by a linear model regressing unit activity in**
1772   **PMd against reaction time for the fixed duration task only increases after the go**
1773   **cue.** Red traces represent average fraction of variance for rightward choices and blue
1774   traces for leftward choices ± SEM (shaded areas). Across the population, neural
1775   activity only becomes a reliable RT predictor on or after the time of the go cue.
1776   Magenta and cyan lines (highly overlapping) show results from a model trained on
1777   shuffled data as a control. Red (Blue) dots above the x-axes denote time points for
1778   which the explained variance was significantly different from baseline (defined as the

40

1779   average for [-100, 200] aligned to targets onset) for T1 (T2) according to Wilcoxon
1780   signed-rank test (p<0.01 Holm-Bonferroni correction for multiple comparisons).
1781   Median RTs for fixed duration task monkey H: 361 ms, monkey F: 424 ms.
1782   **b) Fraction of variance explained by a linear model regressing unit activity in**
1783   **M1 against reaction time for the fixed duration task only increases after the go**
1784   **cue.** Same as a) for M1. Figure conventions as in **a)**
1785   **c) Fraction of variance explained by a linear model regressing unit activity in**
1786   **PMd against reaction time for the variable duration task only increases after the**
1787   **go cue.** Figure conventions as in **a).** Median RTs for variable duration task monkey
1788   H: 335 ms, monkey F: 427 ms.
1789   **d) Fraction of variance explained by a linear model regressing unit activity in**
1790   **M1 against reaction time for the variable duration task only increases after the**
1791   **go cue.** Figure conventions as in **a)**
1792   **e)-h) Same as a)-d) for hand peak velocity.** Across the population, neural activity is
1793   a poor predictor of hand peak velocity throughout the trial; a slight increase in
1794   variance explained occurs only around reach initiation.
1795
1796
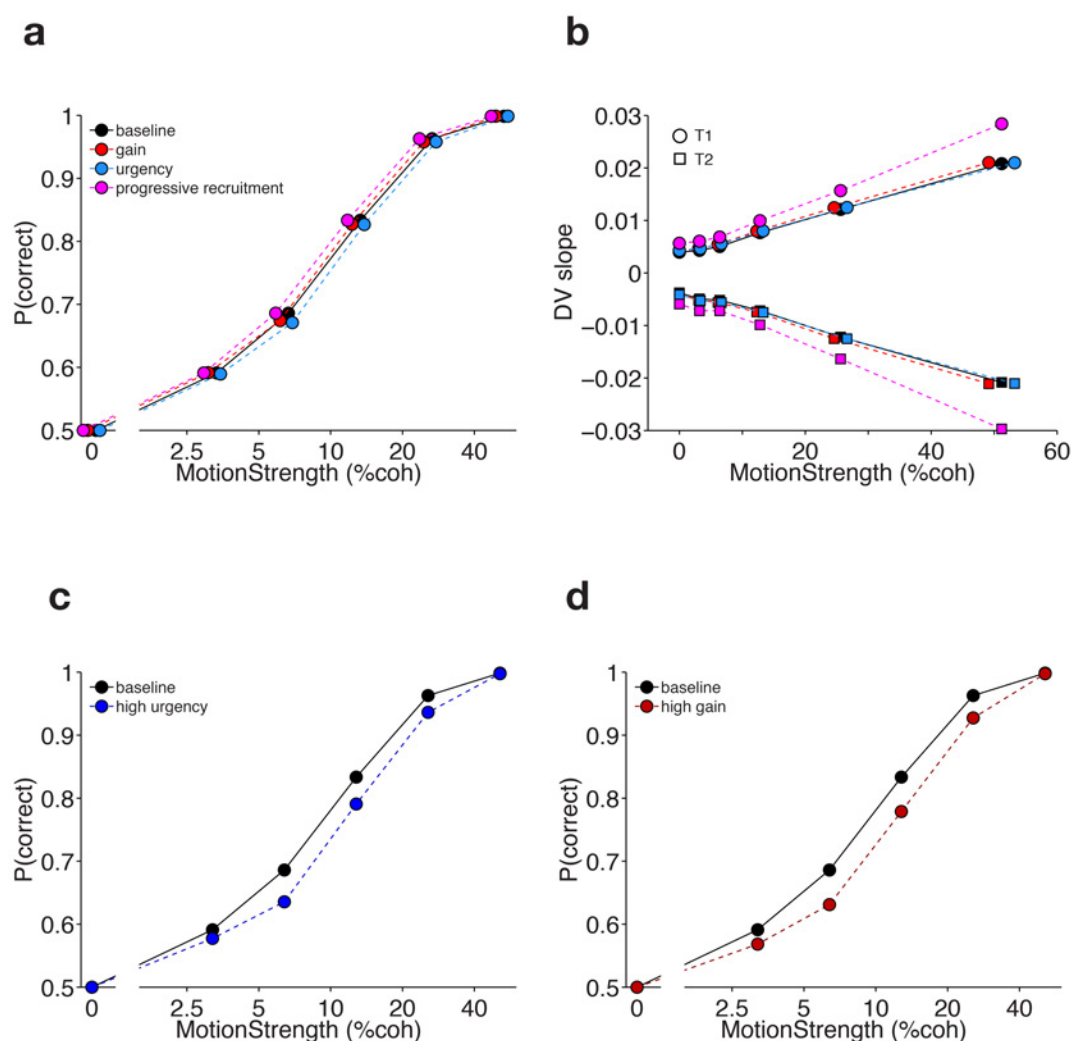
1797
1798   **Figure 5 – Modeling results suggest that the progressive recruitment model can**
1799   **explain the increase in the DV slopes for the variable duration task.** When the
1800   parameters of the urgency, gain, and progressive recruitment models are adjusted to
1801   match the psychometric function under two task conditions (**a**), only the progressive

41

1802   recruitment model could replicate the increased DV slopes observed in the data (**b**).
1803   Because the curves were highly overlapping, data points in (**a**) were offset on the x-
1804   axis by multiplying the x-coordinates by a factor c for each curve ($c_{baseline} =$
1805 1.04, $c_{gain} = 0.96$, $c_{urgency} = 1.08$, $c_{PRM} = 0.92$) to aid interpretation. Same
1806   procedure was performed in (**b**) with $c_{baseline} = 1$, $c_{gain} = 0.96$, $c_{urgency} =$
1807 1.04, $c_{PRM} = 1$. Increasing urgency or gain to match the increased DV slopes leads
1808   to significant changes in the psychometric function, inconsistent with the observed
1809   data (**c** and **d**).
1810
1811
1812
1813

42

1814
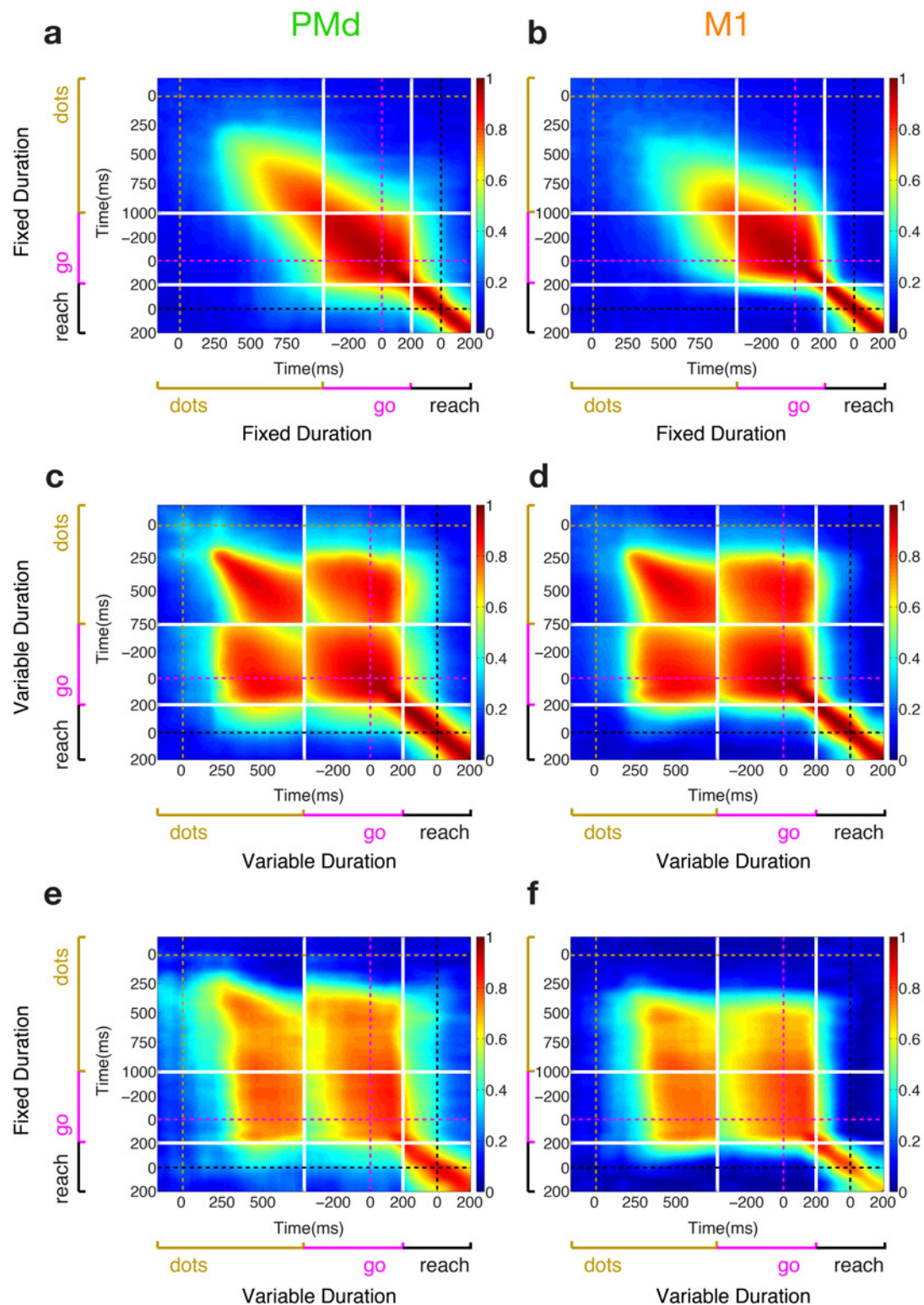
1815
1816
1817 **Figure 6 – Stability of choice representation during dots is dependent on the**
1818 **statistics of stimulus duration (pooled results across 2 monkeys).**
1819
1820 **a) Choice representation only becomes stable late in the dots presentation period**
1821 **in the fixed duration task.** Heat map shows the dot product of the choice vector
1822 (vector of beta values for choice) across time. Vectors were obtained using 50 steps of

2-fold cross-validation. Warm colors correspond to very high overlap between vectors whereas cool colors denote little projection between vectors. In PMd (left panel) choice representation becomes stable ~600 ms after stimulus presentation. In M1 (right panel) this phenomenon occurs even later around ~750 ms. Note how broadly stable the choice signal is during the delay period and how locally stable it is around the reach. White solid lines denote the separation of epochs (dots end, and go cue +200 ms), golden, magenta and black dashed lines mark the dots onset, go cue and reach initiation, respectively. Data from both monkeys. **b)** Same as **a)** for M1.

c) Choice representation becomes stable very early in the dots presentation period in the variable duration task. Heat map shows the dot product of the choice vector (vector of beta values for choice) across time. The choice signal is already very stable only 300 ms after the stimulus presentation both in PMd (left panel) and M1 (right panel). Unlike in **a)** and **b),** the pre-go period in the variable duration task overlaps with the dots period because of the absence of a delay period; thus correlations in the off-diagonal quadrants should be interpreted with caution since the same data can be correlated against themselves. Figure conventions as in **a)**. Data from both monkeys. **d)** Same as **c)** for M1.

e) Choice representation is stable across tasks. Heat map shows the dot product of the choice vector (vector of beta values for choice) across time between the fixed duration task (y-axis) and the variable duration task (x-axis). Note that the representation of choice in the second half of the dots presentation and delay period on the fixed duration task strongly overlaps with the early choice representation in the variable duration task. Figure conventions as in **a)**. Data from monkey F. **f)** Same as **e)** for M1.
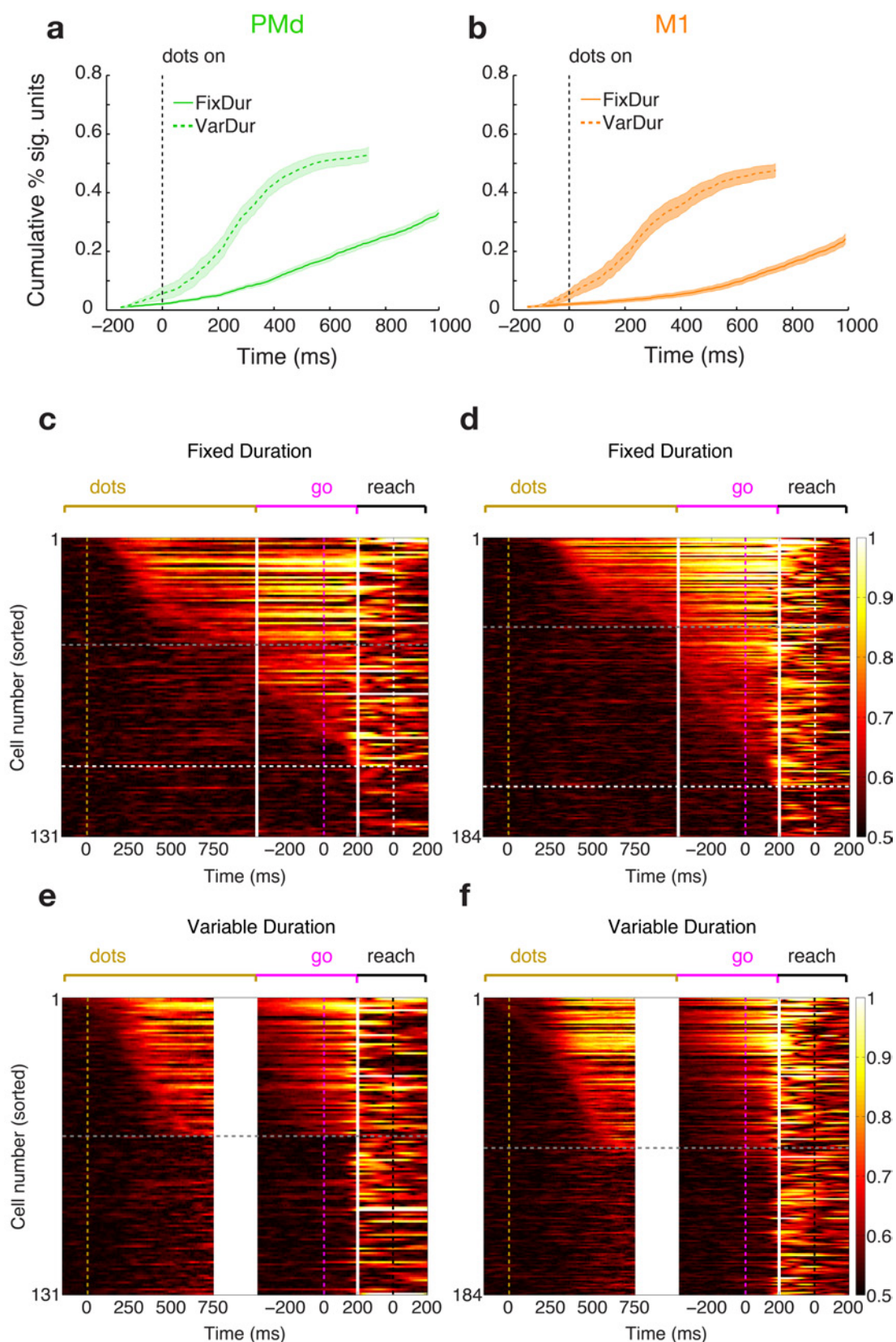
Figure 7 – Recruitment of choice predictive cells accelerates for both brain areas under uncertainty conditions.

a) Fraction of units carrying significant choice signals increases faster in the variable duration task. The cumulative fraction of units with significant choice

1855   signals is plotted as a function of time aligned to dots onset for PMd. Solid line shows
1856   the results for the fixed duration task and dashed line the variable duration task.
1857   Shaded areas denote ± SEM (across sessions). Data from both monkeys. **b)** Same as
1858   **a)** for M1.
1859   **c) Individual unit choice predictive activity is stable during dots presentation**
1860   **and builds up slower in the fixed duration task.** Area under ROC traces for all
1861   units recorded in one session in PMd. Traces we sorted by onset of significant choice
1862   modulation during the dots presentation (one row for each unit). White solid lines
1863   denote the separation of epochs (dots end, and go cue +200 ms); golden, magenta and
1864   black dashed lines mark the dots onset, go cue and reach initiation, respectively.
1865   Horizontal dashed gray line separates cells with significant choice modulation during
1866   dots (above) from cells with significant choice modulation that only starts during the
1867   delay period. Horizontal dashed white line separates the latter group from the
1868   remainder of the population (below). Data from monkey F. **d)** Same as **c)** for M1.
1869   **e) Individual unit choice predictive activity is stable during dots presentation**
1870   **and builds up faster in the variable duration task.** Figure conventions as in **b)**.
1871   Data from monkey F. **f)** Same as **e)** for M1.
1872
1873
1874
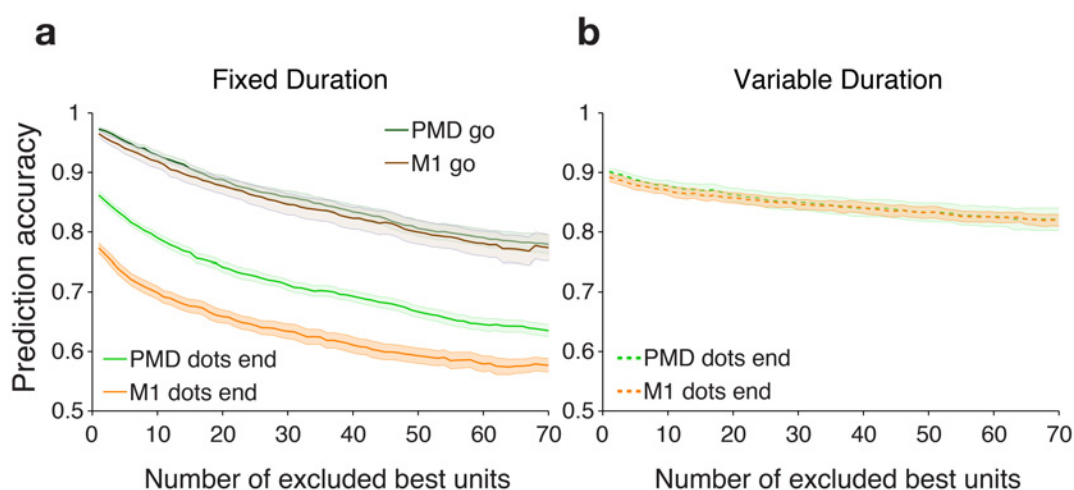
1875
1876
1877
1878
1879   **Figure 8 - Choice signal is robust and distributed across the population of cells in**
1880   **both areas and both tasks (pooled results across 2 monkeys).**
1881
1882   **a) Choice signal is robust in the fixed duration task.** Average prediction accuracy
1883   curves for PMd (green) and M1 (blue) ± SEM (shaded areas) as a function of the
1884   number of best units excluded for the fixed duration task. The unit dropping curves
1885   were calculated for two separate time points: end of dots presentation (light shades)
1886   and go cue presentation (dark shades) Curves were calculated for each session/area
1887   separately and then averaged across sessions. The decay in performance is smooth,
1888   demonstrating that the choice signal is distributed across many cells. As expected
1889   from figure 2 a), the initial accuracy for the go cue period is higher than for the end of
1890   dots.
1891   **b) Choice signal is extremely robust in the variable duration task.** Same as **a)** for
1892   variable duration task. The choice signal is even more robust in this task as evidenced

1893   by the very small decline in prediction performance (<10%) after dropping the 70 best
1894   units. Figure conventions as in **a)**. The end of dots and go cue coincide in this
1895   version of the task so only one curve is shown for each area.
1896